Condition monitoring of journal bearings based on acoustic emissions: A state-of-the-art review

Jiaojiao Ma[1], Jiefei Yu[1], Xianwen Zhou[1], Fengshou Gu[2], Lingli Jiang[1,✉], Xuejun Li[1]

Cite this article: Ma JJ, Yu JF, Zhou XW, et al. *Friction* 2026, **14**(1): 9441080. https://doi.org/10.26599/FRICT.2025.9441080

ABSTRACT: This article provides a thorough review of the advancements in acoustic emission (AE) technology used for monitoring journal bearings. First, the AE sources generated from journal bearings under different lubrication regimes are classified and discussed. Next, a comparative analysis of parametric analysis, waveform, and artificial intelligence recognition methods for bearing AE signal analysis is conducted, highlighting their respective principles, pros and cons, and applications. Additionally, an overview of physical models representing AE waves on relatively sliding surfaces is provided from the wave generation mechanism perspective, and each model's applicable conditions are compared. Finally, an in-depth discussion is presented, and future research directions are highlighted.

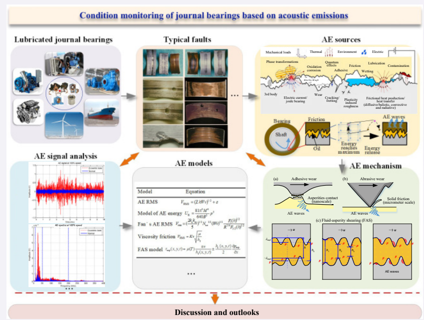

KEYWORDS: journal bearing; acoustic emission; condition monitoring; acoustic emission (AE) modeling; signal processing

1 Introduction

Research on condition monitoring and early fault diagnosis of lubricated rotating machinery has increased significantly over the past several decades. The relative sliding components, such as gears, bearings, seals, etc., are separated by a lubricating film that minimizes friction and wear [1–5]. Among these critical parts, journal bearings—used in internal combustion engines, steam turbines, compressors, and ship propulsion shafts—have been widely used in rotating machines as the most typical lubricated components [6–8] due to their increased rotation accuracy and extended service life [9]. More recently, journal bearings have also been incorporated into the planetary gearboxes of advanced aircraft engines and wind turbines [10]. In practice, journal bearings often operate under heavy loads or at high rotational speeds for extended periods. As a result, friction and wear on journal bearings operating under such extreme conditions are inevitable and must be closely monitored.

The unique structure of journal bearings dictates that the condition of the lubricating oil film is crucial for determining the lubrication regimes and evaluating the bearing's early faults. According to statistical data, faults related to the oil film account for up to 70% of journal bearing failures [11]. When lubricant quality deteriorates due to contaminants, the tribo-film can partially rupture, and consequently, adhesive wear, abrasive wear, surface fatigue wear, and elastic or plastic deformation will occur step by step [12–15]. Therefore, practical techniques are urgently needed to identify these faults. Traditional condition monitoring techniques include wear debris, thermography, vibration, and spectrometric oil analysis [16–18]. Impedance and ultrasonic technologies are also widely used to measure the oil film thickness between sliding surfaces [19–21]. Each method has advantages and limitations when applied to the condition monitoring of journal bearings. The limitation of temperature analysis lies in the slow diffusion of heat, which reduces its sensitivity for the early fault. Vibration analysis is the most widely used method in rotating machinery fault diagnosis because of its nondestructive test (NDT) capabilities [22–24]. However, detecting the early stages of weak abrasive wear in journal bearings and capturing high-frequency fault information at the initial stages are challenging. Oil analysis is the most accurate method for detecting oil contaminants, but it is typically limited to offline measurements, which involve considerable time and equipment costs. Advanced spectrometric oil analysis has facilitated online monitoring of wear debris by integrating a complex lubrication monitoring system. However, this method does not provide comprehensive information on the condition and characteristics of degraded lubricants. Unlike traditional impedance methods, ultrasonic detection does not require modifications to the friction pair surfaces. Additionally, its penetration capability addresses the limitations posed by the light transmission requirements of optical methods. While ultrasonic technology is primarily used for the nondestructive testing of materials and components, it has certain limitations in monitoring the progression of faults over time.

These methods have certain limitations in real-time monitoring of journal bearing faults, particularly in capturing early fault

[1] School of Mechatronic Engineering and Automation, Foshan University, Foshan 528000, China. [2] Centre for Efficiency and Performance Engineering, University of Huddersfield, Queensgate HD1 3DH, UK.

✉ Corresponding author. E-mail: linlyjiang@163.com

Received: February 25, 2024; Revised: December 30, 2024; Accepted: February 17, 2025

Nomenclature

A_n	Amplitude of AE signals	k_m	Gain of the ae measurement system
A_0	Apparent deformation area	M	Hertzian contact modulus
a_n	Asperities radius	N	Average number of contact zones
B	Coefficient obtained by $b = (1 + r_1/r_2)/r_1$	N_{tot}	Total number of contacting asperities
D_s	Density of asperities	$\dot{N}_{AE}$	Count rate of AE
D_{SUM}	Total number of asperities per unit area	P_p, P_e	Plastic load and elastic load
d	Distance between the average planes of the surfaces	p	Average pressure
E	Young's modulus	R_1, R_2	Radii of the spherical shapes as the contacted asperities
F	Average friction force	R, R_s	Curvature radii and the equivalent curvature radii of contacting asperities
F_0	Calculation coefficient with a force dimension	R'	Hertzian curvature
F_{tot}	Total force pressing the surfaces	S	Distance between tape and specimen
F_N	Normal load	U_E, $\dot{U}_E$	Energy and energy release rate of the elastic deformation
G	Parameter of the surface's fractal roughness	V_{RMS}	Voltage of ae signals
H	Hardness of the material	V	Volume of material lost during the abrasion process
h_f	Lubricant film thickness	v	Speed of the relative sliding
h_0	Nominal height	W_r, $\dot{W}_r$	Energy and power of the material removal
I	Area moment of inertia	W	Normal load
K_c	Electromechanical conversion factor of a piezoelectric transducer	U_{sum}, $\dot{U}_{sum}$	Total energy and energy release rate of the asperity's deformation
k	Wear coefficient	Z	Impedance of the measurement system
k_e	Portion of the elastic strain energy converted to AE pulses	z_s	Height of asperities
Greek symbols			
α	Ratio of standard deviations	μ	Viscosity of the lubricant
β	Coefficient of temperature	τ	Shear stress
δ_{asp}	Time-varying height	φ	Standardized height distribution
ε	"Noise" in the system	ζ_i	Random initial phase angles
σ	Standard deviation of random functions $z(x)$	χ_i, $\chi_{mid,i}$, $\Delta\chi_i$	Spatial frequency, center frequency, and width of each frequency interval
Abbreviations			
AE	Acoustic emission	k-NN	k-nearest neighbors
ANN	Artificial neural networks	LSTM	Long short-term memory
ANN–GA	Artificial neural networks with genetic algorithms	ML	Mixed lubrication
BL	Boundary lubrication	NDT	Nondestructive test
CNN	Convolutional neural networks	PSD	Power spectral density
CWT	Continuous wavelet transform	RMS	Root mean square
DNN	Deep neural networks	RUL	Remaining useful life
FAS	Fluid–asperity shearing	SNR	Signal-to-noise ratio
HL	Hydrodynamic lubrication	SVM	Support vector machine

information and tracking dynamic fault progression. The acoustic emission (AE) technique, as an NDT method, is sensitive to the rapid release of local energy during the processing of elastic and plastic deformation, e.g., sliding friction, material delamination, crack growth, and fluid friction [25–27]. In the 1950s, Joseph Kaiser pioneered AE technology to investigate the "sounds" generated during tensile tests on metallic samples [28]. The development of modern AE instruments has led to extensive, in-depth research on AE source mechanisms, wave propagation, and acoustic emission signal analysis. Consequently, the application scope of AE technology has significantly expanded, particularly in the condition monitoring of gears, bearings, seals, and other lubricated rotating machinery [29–32]. For journal bearings, the first AE signal analysis was performed in 1985 by Sturm and Uhlemann [33]. Various studies have subsequently introduced the superiority of the AE technique in the application of journal bearing fault diagnosis [34, 35].

In this work, various failure modes of journal bearings are investigated to analyze the effective application of AE technology in journal bearing condition monitoring. It introduces appropriate signal processing methods for extracting fault features across different failure types by examining the correlation between AE sources and specific failure modes in journal bearings. A comprehensive review of recent advancements in AE models is presented, with a focus on the mechanical processes and physical principles involved. Additionally, by comparing data-driven models with theoretical models, the advantages and challenges of AE technology in diagnosing journal bearing faults are highlighted.

The rest of this work is organized as follows. The sources of the AE signals from the journal bearings and the fault modes of the bearings are presented in Section 2. The processing techniques for the AE signals and the derived AE models are introduced in Sections 3 and 4, respectively. An in-depth discussion of the advantages and challenges associated with applying AE technology in the condition monitoring of journal bearings is provided in Section 5. The main development trends of the application of AE technology to journal bearings are also analyzed. Finally, Section 6 summarizes the conclusions regarding the use of AE techniques for the condition monitoring of journal bearings.

2 Source of AE signals related to journal bearings

2.1 Classification of journal bearing failures

A lubricated journal bearing generally consists of three main parts: the journal, the bearing, and the oil film. During operation, the surfaces of the journal and bearing slide over a thin oil film, which reduces friction and removes heat from the bearings. The lubrication regime depends on the thickness of the oil film, which varies due to the combined effects of the load, rotating speed, and rheological properties of the lubricant. In the hydrodynamic lubrication (HL) regime, the relatively sliding surfaces are entirely separated by the oil film. In the mixed lubrication (ML) regime, there is partial contact between solid surfaces, while in the boundary lubrication (BL) regime, the relative sliding surfaces come into direct contact with each other. Journal bearing failures can generally be caused by many factors [36]. The transition between lubrication regimes is the primary reason for the different degrees and forms of journal bearing failure, particularly under inadequate lubrication conditions [37].

Practically, the incipient failure of journal bearings occurs in an entire film lubrication regime, such as friction wear caused by the elastic deformation of asperities on sliding surfaces [40, 41], as well as cavitation corrosion resulting from cavitation phenomena and water contamination. The lubricant further deteriorates as the lubrication regime transitions to the ML and even BL regimes, resulting in faults. For example, failures of journal bearings in the IC engine crankshafts can generally be categorized into tribological failures and mechanical failures [38]. The former comprises abrasive wear from scratches and scoring, adhesive wear caused by wiping and seizure, surface fatigue wear, flow and discharge cavitation wear, corrosive wear, and erosive wear. The latter primarily involves plastic deformation and fracture. In addition, the faults of journal bearings in other machines manifest as fretting, electrical pitting, chemical corrosion, thermal fatigue, and other issues [42]. The diagram in Fig. 1 illustrates the predominant types of faults and their corresponding occurrence percentages. The main failures in crankshaft bearings and industrial applications are abrasive and adhesive wear [38, 39]. Figure 2 shows the failure macrograph of the journal bearings.

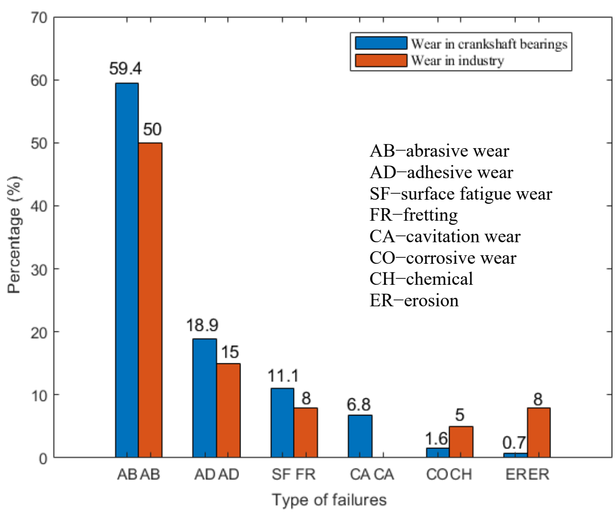

Fig. 1 Percentages of failures in bearings and industry [38, 39].

2.2 Source of AE signals from journal bearings

Acoustic emission refers to the phenomenon where strain energy is quickly released as elastic waves generated by the deformation or cracking of materials or components under stress [43–46]. The elastic wave source directly related to the deformation or fracture mechanism is commonly referred to as a typical AE source. Other sources indirectly associated with deformation or fracture mechanisms are referred to as secondary AE sources, such as fluid leakage, friction, impact, and combustion [35, 47–49]. Owing to the multiphysical nature of tribological interactions, these behaviors involve mechanical contact and the application of various loads (mechanical, thermal, electrical, and environmental) on two surfaces with different roughnesses [50] and material microstructures [51], as shown in Fig. 3. On the basis of molecular lattice theory, the mechanism underlying AE generation from relative sliding surfaces is demonstrated in Fig. 4.

For journal bearings, the AE sources critically depend on the condition of the lubricant tribo-film. On the basis of the Stribeck curve illustrated in Fig. 5, the AE sources mainly include friction, abrasive wear, adhesive wear, cyclic fatigue, and cracks in both BL and ML regimes [53, 54]. Figure 6 shows the AE response generated from adhesive wear, abrasive wear, and fluid–asperity shearing, which are typical AE sources in journal bearings. The occurrence of adhesive wear is attributed to adhesion and breakage at the contact interface. The AE mechanism is related mainly to plastic deformation and atomic movement processes, which depend on the Frank–Read mechanism. With the appearance of twinning and grain boundary sliding, there is an increase in the accumulation of wear elements on the sliding surfaces, which can intensify adhesive wear by forming transfer particles. Therefore, the primary cause of AE wave generation resulting from adhesive wear lies in the presence of these wear elements and transfer particles, as shown in Fig. 6(a). AE sources are related to damage mechanisms associated with the origin and accumulation of microscopic defects, crack initiation and propagation, and corrosion-induced cracking. Generally, the mechanisms of adhesive wear and abrasive wear tend to coexist. Figure 6(b) illustrates the AE source during abrasive wear. The abrasive wear process involves shear fracture and plastic deformation on sliding surfaces in relative motion. Compared with plastic deformation, shear fracture releases more strain energy and represents a nonhomogeneous deformation process that occurs rapidly. Consequently, shear fracture is the primary source of AE waves generated from abrasive wear [37]. The AE source in the HL regime, where an oil film completely separates the relative sliding surfaces, is particularly interesting. Figure 6(c) presents the process of AE wave generation based on three pairs of asperities with different heights on the sliding surfaces. On the basis of the calculation of the shearing force, the sizeable shearing force is caused by a small thickness as the viscosity and speed are constant, as illustrated by the symbol *F*. With the variation in shear force, the energy in the asperities progressively accumulates and subsequently releases, leading to the generation and propagation of AE waves, which is visually represented by the presence of half-red circles in the figure. On the basis of the AE technique, this conclusion has practical implications for estimating initial failures occurring in journal bearings.

The occurrence of wear and metal wipes in journal bearings, particularly common bearing wear caused by the gradual scraping

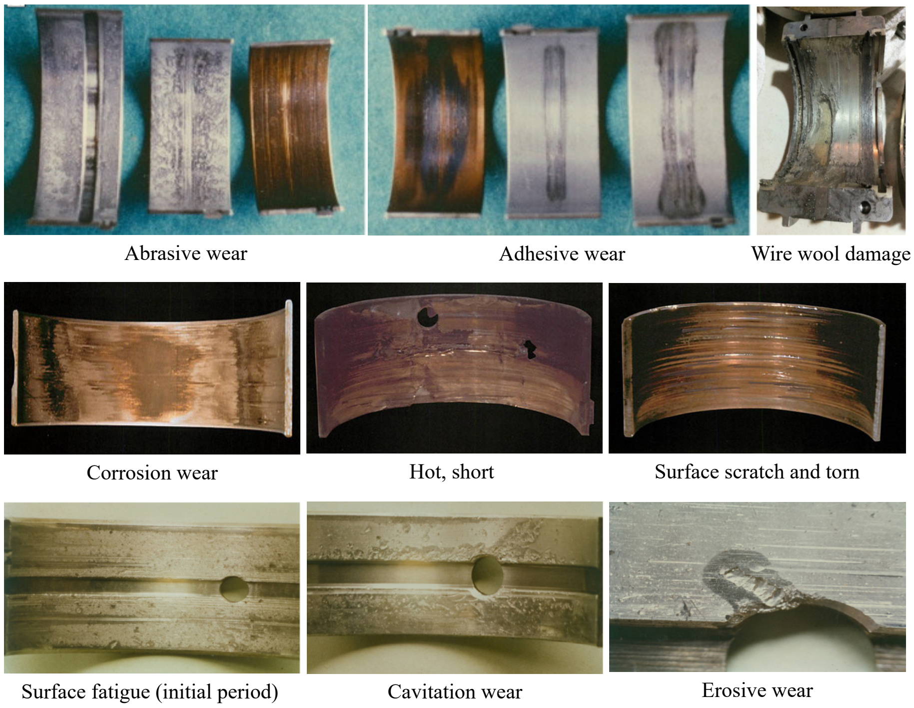

Fig. 2 Failure forms of journal bearings. Reproduced with permission from Ref. [38] for (a), (b), and (h–j), © Elsevier Ltd. 2014.

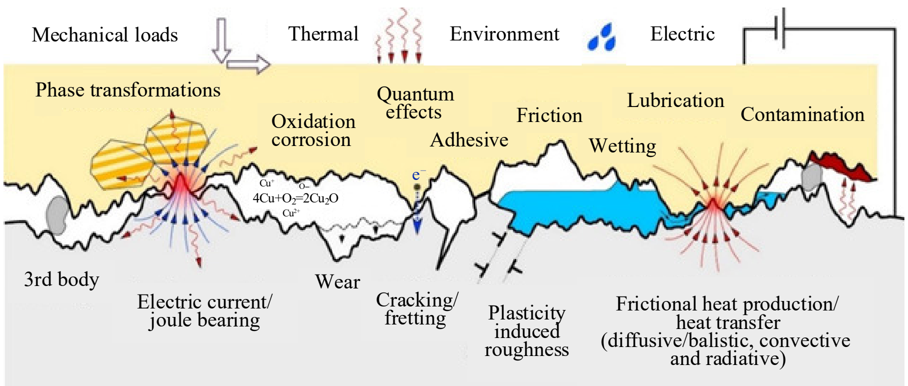

Fig. 3 A scheme representing multiphysical nature of tribological interactions. Reproduced with permission from Ref. [51], © Elsevier Ltd. 2018.

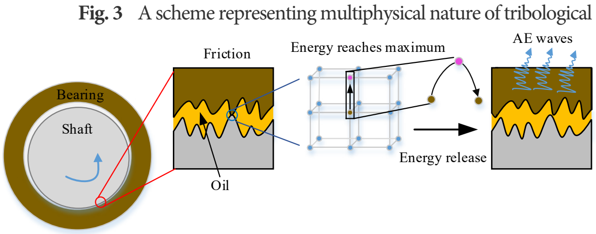

Fig. 4 AE response from relative sliding surfaces [52].

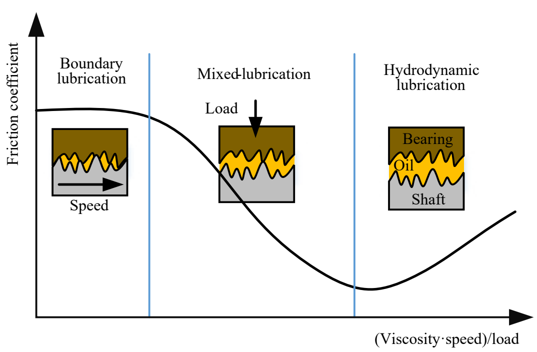

Fig. 5 Stribeck curve.

of the bearing liner during start-up and shutdown, is a prevalent issue resulting from direct contact between the journal and bearing surfaces. Therefore, the research has shifted toward the states of the ML and BL regimes, which result from the contact processing of sliding surfaces when the tribo-film ruptures. Regarding the impact of the absence of a lubricating oil film on AE sources, Bonnes et al. [56] conducted a study using a ball-on-rod testing platform to examine the relationship between AE and wear under dry friction and lubricated sliding conditions. Their research confirmed that AE generated under oil-lubricated conditions is associated with the adhesion process, whereas in the absence of lubrication, AE results from abrasive wear. Sturm and Uhlemann [33] employed the AE technique to investigate the lubrication state of plain bearings, demonstrating its potential for detecting the transition from the fluid to the ML regime. Similarly, Ziegler et al. [57] examined the AE sources in sliding bearings subjected to varying loads and temperatures. Their findings revealed that, compared with hydrodynamic friction, solid friction had a more significant effect on the AE response. Couturier and Mba [58] explored the relationships between rotating speed, load, film thickness, and the AE response. Furthermore, Ziegler et al.

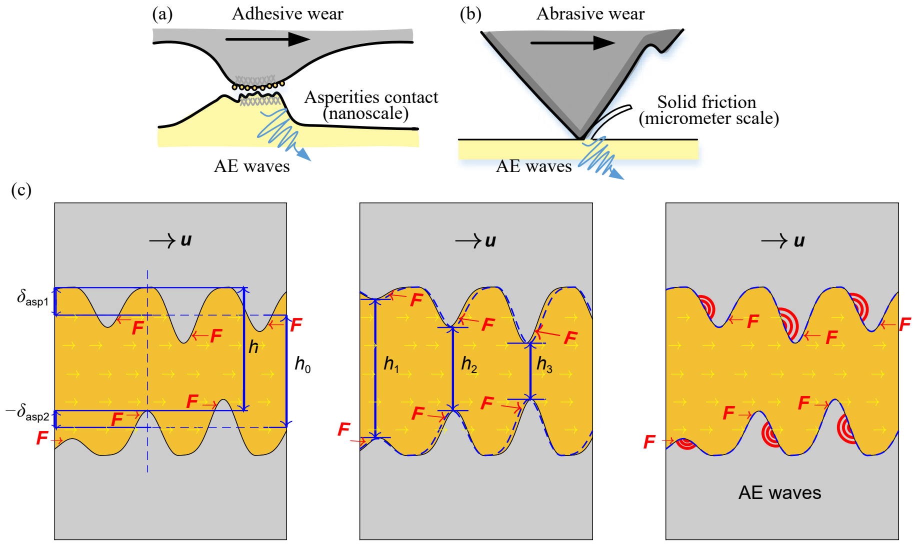

Fig. 6 AE sources from (a) adhesive wear, (b) abrasive wear, and (c) fluid–asperity shearing (FAS). Reproduced with permission from Ref. [37] for (a, b), © Elsevier Ltd. 2012; from Ref. [55] for (c), © Elsevier Ltd. 2021.

[59] examined the influence of the Sommerfeld number on the AE response, highlighting the clear effect of shear rate intensity on AE activity. Albers and Dickerhof [60] focused on AE generated by solid-body frictions in journal bearings and concluded that the AE characteristics were particularly sensitive to high-frequency components. Nagata et al. [61] conducted start–stop tests on plain bearings made from various materials in crankshafts, assessing the role of AE in condition monitoring of lubricated bearings. In another study, Bergmann et al. [62] investigated the mechanisms of friction and wear, demonstrating the applicability of several AE evaluation parameters that exhibited a strong correlation with these phenomena. Schnabel et al. [63] examined the dependency of AE response on increasing speed and contact time depending on the Hertzian impact and tensile tests. They reported that the key temporal dependencies of AE were related to contact time, event frequency, and AE amplitude. Additionally, Hu et al. [64] extensively investigated the influence of the microscopic morphology of relative sliding surfaces on the AE response. They reported that the primary AE source was the summit of the upper component of a bi-Gaussian stratified surface when the relative sliding surfaces made contact.

In addition to operational conditions, the properties of the lubricant play a crucial role in the formation of the tribo-film, which can significantly influence the wear process and potentially lead to damage in both the journal and the bearing. Factors such as the temperature and contamination level of the lubricant also significantly affect this process [65]. Towsyfyan et al. [66] conducted experiments on a rotor-bearing rig using lubricants with three different viscosities and investigated the AE signals generated from asperity contacts in mix-lubrication. Under identical loads and speeds, Mokhtari et al. [10] investigated the correlation between changes in oil viscosity and the AE response. Moshkovich et al. [67] conducted specialized studies to achieve a transition from elastic–hydrodynamic lubrication to BL regions and investigated the interaction between friction and AE parameters for materials with varying stacking fault energies. The primary cause of early journal bearing failure is lubricant contamination, which adversely affects a bearing's performance over a long period of time [68]. The classical contaminants are particle contamination and water contamination. The presence of unwanted particles in the oil film regime can cause surface damage to both the journal and the bearing [69]. Poddar and Tandon [11] investigated the impact of lubricants contaminated with particles of varying sizes and volumes on the behavior of journal bearings. They quantified the correlation between these contaminants and AE responses through a detailed evaluation. Their findings indicated that the primary AE source was three-body abrasion caused by particle-contaminated bearings.

In the HL regime, researchers have also conducted studies to analyze the AE sources at the relative sliding interfaces. Towsyfyan et al. [70] illustrated the AE energy discharge across different lubrication regimes in mechanical seals. They reported that viscous friction was the primary source of AE signals when the surfaces of the mechanical seals were fully separated by the fluid. Additionally, Wei et al. [71] analyzed the AE responses at the lubrication interface between the engine ring and liner and reported that the AE behavior was generated by the fluid-asperity shearing process. For journal bearings, Mirhadizadeh and Mba [74] performed a series of tests to assess the acoustic emission activity in a hydrodynamic bearing under various operating conditions, establishing an initial correlation between the AE response and these conditions. Ma et al. [55] investigated AE generation in the HL regime using a rheometer rig for testing. They concluded that the AE response was due primarily to dynamic fluid-asperity shearing during the operation of journal bearings in the HL regime.

According to previous studies, the correlation between AE sources and journal bearings' conditions is summarized in Table 1. This research focused primarily on the impact of operating conditions on the BL and HL regimes, utilizing AE techniques. The information extracted from the ML regime and lubricant contaminants plays a pivotal role in condition monitoring and early fault diagnosis of journal bearings in practical applications. Therefore, acquiring this critical information requires further research and the development of advanced techniques and methodologies.

3 AE signal analysis and processing

3.1 Characteristics of AE signals

The waveforms of AE signals can be classified into two types: burst AE signals and continuous AE signals, as shown in Fig. 7. The former is sporadic and temporally separable, whereas the latter exhibits continuous variations over time in the case of

Table 1 AE generated from journal bearings

Lubrication condition	Source for AE	Effect parameter	Refs.
Boundary lubrication	Solid friction, surface fatigue wear, fracture, hot short	Rotating speed, load, viscosity	[56, 60, 61, 63, 72]
		Surface materials	[62, 64, 67, 73]
Mix-lubrication	Solid friction, fluid friction, fretting, abrasive wear, flow cavitation, discharge cavitation, plastic deformation	Rotating speed, load, viscosity	[33, 53, 57, 64]
Hydrodynamic lubrication	Fluid friction, plastic deformation, fluid-asperity shearing, corrosive wear, erosive wear	Rotating speed, load, viscosity	[10, 55–57, 74–77]
		Lubricant contaminations	[11, 65, 69]

persistent AE signals. Initially, AE signals were utilized to detect faults arising from sliding friction or wear [78–81]. For journal bearings, poor operation may result in the generation of bursts and continuous AE signals. The Hertzian contact stress leads to burst AE signals, which are caused by the relative motion and rubbing between the relative sliding surfaces of the journal and bearing, and failures, including surface cracks, adhesive wear, abrasive wear, indentations, grooves, bites, etc., which occur due to overloads and inadequate lubrication. In addition, the surface of hard edges, contaminated particle lubrication, and pitting corrosion caused by the shaft current produce burst AE signals. The continuous AE signals generated by journal bearings are attributed primarily to boundary lubrication and dry friction, which occur due to the failure of the lubricating oil film and severe contamination in the lubricants.

AE signals collected through AE technology contain fault information that can be used to monitor and diagnose the lubrication condition of sliding bearings [42]. The AE sources generated within journal bearings release energy in the form of pressure waves, which propagate through the solid surface and can be detected by AE sensors, as shown in Fig. 8. Practically, the sensors exhibit unique characteristics on the basis of their specific structure and material properties. The frequency range of AE waves is broad, spanning from infrasonic to ultrasonic frequencies, ranging from several hertz (Hz) to several megahertz (MHz). The amplitude varies greatly, ranging from microscopic dislocation rotation to large-scale macroscopic fracture. The sensor output can range from a few μV to hundreds of mV. However, most signals are weak vibrations that require highly sensitive sensors for detection. With the most sensitive sensors available, surface vibrations as small as 10^{-11} mm can be detected

Fig. 7 Waveform of AE signals: (a) burst AE signal; (b) continuous AE signal.

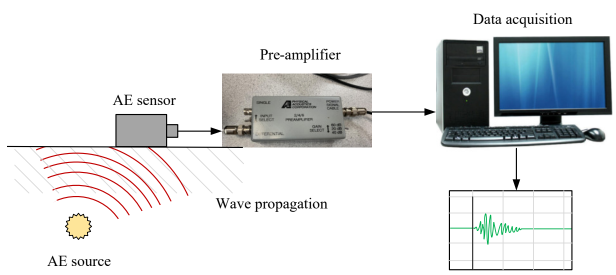

Fig. 8 Acoustic emission detection system.

[82]. In addition, the propagation of AE waves from the source to the surface-mounted sensors can alter the characteristics of these waves. Signal attenuation is an inevitable phenomenon during transmission due to material damping, frictional losses, and dispersion. Therefore, selecting appropriate signal processing methods is critical for accurate signal analysis.

3.2 Methods of AE signal analysis

Although the acquired AE signals exhibit an enhanced signal-to-noise ratio (SNR) owing to the continuous optimization of preamplifiers and sensors, information extraction for fault detection in journal bearings is challenging in boisterous environments. Therefore, the AE signals need to be preprocessed before extracting the features. Extensive research has been dedicated to the effective processing of original AE signals, and various techniques for processing and analyzing AE signals have been established. To date, analysis techniques for AE signals generated from the relative sliding surfaces in journal bearings are summarized from the following three perspectives.

3.2.1 Parametric analysis method

Conventional methodologies for analyzing AE signals include parametric analysis and waveform analysis. The parametric analysis method encompasses the peak amplitude, ring count, event count, duration, and door sill value, as illustrated in Fig. 9. In addition, the statistical magnitude can be utilized for the analysis of AE signals, including parameters such as the mean, root mean square (RMS), standard deviation, energy, skewness, and kurtosis in the time domain, as well as the mean frequency, median frequency, and peak frequency in the frequency domain [83–85, 117]. The formulas for these features are summarized in Table 2.

In the time domain, the AE RMS is frequently employed to analyze the AE signals generated from journal bearings during feature analysis [37, 75, 86, 87]. Nagata et al. [61] conducted start–stop tests and seizure tests and reported that the RMS of the AE signals was suitable for the condition monitoring and tribological properties of bearings. Gesella and Murawski [88] carried out journal bearing tests under various shaft speeds and loads and analyzed the characteristics of AE signals, including the

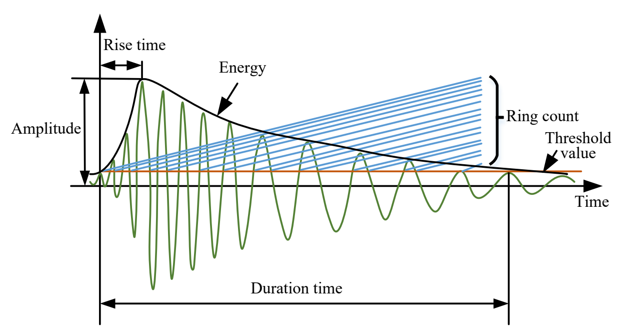

Fig. 9 Parameters of AE waves.

Table 2 Calculations of the main parameters of AE signals [90–93]

AE parameter		Formula	Application in journal bearings
Time domain	Peak amplitude	$y_{\text{peak}} = \max\lvert y(n)\rvert$ where y is the AE signal	Refs. [53, 86, 92, 94–97]
	Mean	$y_{\text{mean}} = \frac{\sum_{n=1}^{N}(y(n))^2}{N}$ where N means the number of the data y	Refs. [80, 98]
	RMS	$y_{\text{RMS}} = \sqrt{\frac{\sum_{n=1}^{N}(y(n))^2}{N}}$	Refs. [37, 53, 61, 75, 76, 86, 87, 92, 94–96, 99–103]
	Entropy	$y_{\text{Entropy}} = -\sum_{n=1}^{N} y_n^2 \log(y_n^2)$	Refs. [52, 103]
	Kurtosis	$y_{\text{Kurtosis}} = \frac{\sqrt{\sum_{n=1}^{N}(y(n)-y_{\text{mean}})^4}}{(N-1)y_{\text{std}}^4}$ where the standard deviation is calculated by $y_{\text{std}} = \sqrt{\frac{\sum_{n=1}^{N}(y(n)-y_{\text{mean}})^2}{N-1}}$	Refs. [52, 103, 104]
	Skewness	$y_{\text{skew}} = \sum_{n=1}^{N}(y(n)-y_{\text{mean}})\frac{3}{(N-1)y_{\text{std}}^3}$	Ref. [92]
Frequency domain	Mean frequency	$y_{\text{mf}} = \frac{\sum_{k=1}^{K} Y(k)}{K}$ where Y means the frequency domain of AE signals $y(n)$; K is the number of spectral lines	Refs. [92, 97, 105]
	Median frequency	$y_{\text{fc}} = \frac{\sum_{k=1}^{K} f_k Y(k)}{\sum_{k=1}^{K} Y(k)}$ where f_k is the frequency value of the kth spectral line	Refs. [52, 92, 104]
	Peak frequency	$y_{\text{PF}} = \max\ P,\ P = \frac{1}{N}\sum_{n=1}^{N} y_n^2$ where P is the power	Refs. [69, 92, 97, 99, 104]

AE RMS and the amplitudes of the AE signals. They also confirmed the effectiveness of the AE technique in monitoring the condition of journal bearings. The relationships between the friction characteristics of journal bearings and features of AE signals, such as the AE RMS, entropy, kurtosis, and median frequency, were estimated by Mokhtari et al. [52]. They concluded that these results can be used to predict the remaining useful life (RUL) of journal bearings. Mirhadizadeh et al. [89] investigated the impact of varying operating conditions on the AE signals generated from hydrodynamic bearings, as shown in Figs. 10 and 11, and highlighted that the power loss is more sensitive to changes in the AE level. Moreover, the parametric analysis method focuses on analyzing the correlation between two variables, including amplitude, duration, energy, RMS, and ring count [63]. By examining the correlation diagram of AE parameters, it is feasible to identify signals with distinct characteristics.

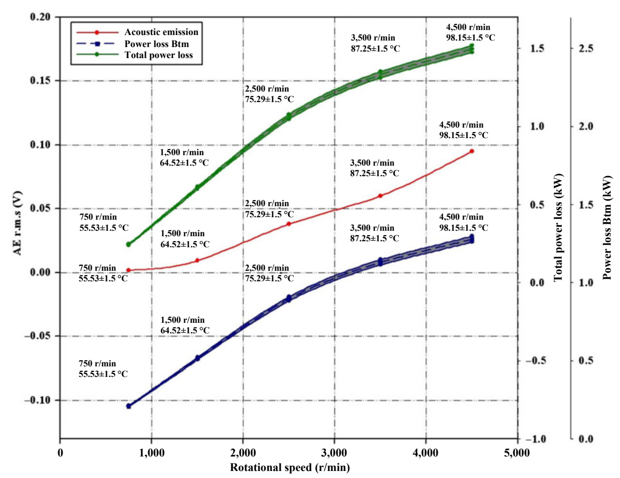

Fig. 10 AE RMS, bottom power loss, and total loss vs. rotational speed and temperature under load of 10 kN. Reproduced with permission from Ref. [89], © Elsevier Ltd. 2010.

3.2.2 Waveform analysis method

The waveform analysis method refers to a signal processing technique that extracts information by analyzing the time-domain waveform or spectral characteristics of AE signals. Currently, waveform analysis relies primarily on the spectral information obtained through the Fourier transform for feature analysis. The frequency band of the AE signals, excluding the spectral parameters listed in Table 2, is also utilized for condition monitoring of the relative sliding surfaces in the frequency domain [106], as illustrated in Fig. 12. Wada et al. [107] investigated the phenomenon of adhesive and abrasive wear and concluded that the frequency band of the AE signals generated by mild adhesive wear was between 2 and 150 kHz, with a peak frequency at 80 kHz; for severe adhesive wear, the frequency band of the AE signals ranged from 1,000 to 1,500 kHz, with a peak frequency at 1,300 kHz. In addition, they verified abrasive wear with an AE spectrum band ranging from 500 to 1,000 kHz, with a peak frequency at 900 kHz. Similarly, severe adhesive wear and abrasive wear were studied by Hase et al. [37], who determined that the frequency ranges associated with these types of wear were 100 to 150 kHz and 200 to 100 kHz, respectively. The AE signals of severe adhesive wear obtained from different studies exhibit the same frequency band. Ramadan et al. [108] investigated various stages of crack wear, including crack initiation, propagation, and even steel failure. The observed frequency band experienced a transition from 300 to 600 kHz and eventually reached 800 kHz. The respective peak frequencies of the three states were measured at 140, 200, and 250 kHz. On the basis of tensile tests, Wada et al. [107] detected two peaks of the AE frequency occurring at 250 and 300 kHz, with the frequency band ranging from 200 to 600 kHz. Yang and Zhou [109] measured the same peak frequency at 250 kHz depending on the tensile test, but the spectral band varied due to the different tested materials. For fatigue testing, the spectral energy of the AE signals generated by long and physically short cracks is focused mainly at 200–400 kHz, and the peak energy occurs at 300 kHz [110]. Additionally, the different conditions of relative sliding surface contact have been

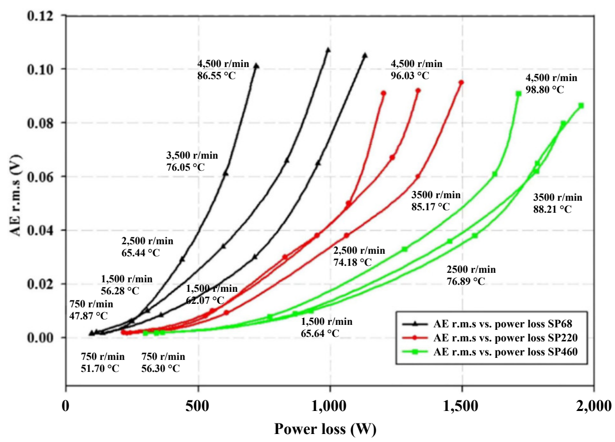

Fig. 11 AE RMS and power loss vs. speed and load (2, 6, and 10 kN) at varying dynamic viscosities. Reproduced with permission from Ref. [89], © Elsevier Ltd. 2010.

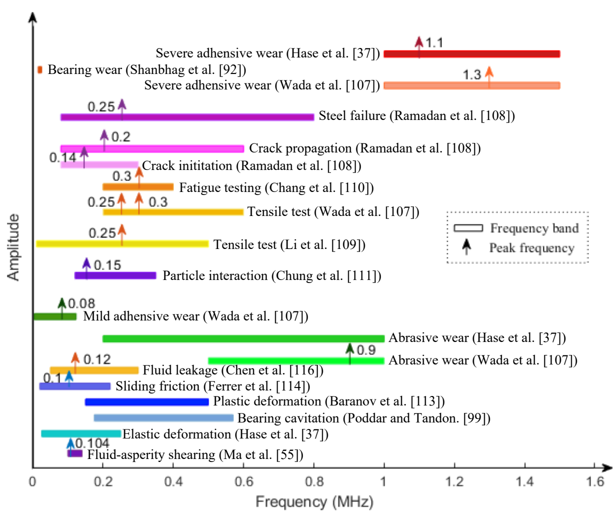

Fig. 12 AE frequency spectra of phenomena generated from the relative sliding surface.

characterized by the spectral bands of the AE signals, involving the particle interaction [111], plastic deformation [112, 113], elastic deformation [107], and sliding friction [114, 115], in which the frequency zone is distributed at 120–350, 150–500, 25–250, and 20–220 kHz. The spectral characteristics of AE signals were investigated by Chen et al. [116] and Ma et al. [55], who reported frequency bands focused on 50–300, 100–140 kHz for fluid leakage and fluid shearing, with peak frequencies observed at 120 and 104 kHz, respectively. The amplitudes of these phenomena, as shown in Fig. 12, reflect the estimated positions derived from the conducted experiments, which may vary depending on operating conditions and materials.

The AE spectral features obtained from the phenomena mentioned above can be used as a robust foundation for evaluating various conditions of journal bearings. The studies involved the condition monitoring of journal bearings on the basis of the spectral bands of the AE signals are summarized in Table 3. The range of the AE frequency band obtained from the journal bearing in the lubricant regime was between 50 and 200 kHz [66, 96, 105]. In the normal lubricant state, Raharjo et al. [95, 96] investigated the AE characteristics generated by the scratched and eccentric bore faults of journal bearings. They reported that a similar frequency band ranged from 10 to 50 kHz, as shown in Fig. 13. Sreedhar and Balasubramanian [118] carried out tests on the lack of lubrication inside the IC engine cylinder and concluded that the AE frequency energy of starvation mainly focused on the spectral band of 20–30 kHz. Poddar and Tandon [99] obtained AE signals generated from journal bearings undergoing vapor cavitation and analyzed the characteristics of the AE signals, including the RMS and energy in the time domain and the peak frequency in the frequency domain. They concluded that the frequency band of the vapor cavitation was 175–570 kHz. Additionally, they carried out experiments on particle contaminants in lubricants on the basis of a journal bearing test rig [11], as illustrated in Fig. 14. They discussed the effects of various particle sizes on the AE response. In Fig. 15, the frequency distance of AE signals was described, and the frequency band of the AE signals caused by particle contamination ranged from 100 to 700 kHz. Shanbhag et al. [92] studied condition monitoring of bearing wear with piston rod seals under varying degrees of wear according to the characteristics of the AE signals, including the AE peak, skewness, and median frequency, and concluded that the frequency band for bearing wear was 15–30 kHz, with a peak

Table 3 AE signal frequencies of phenomena in journal bearings

Phenomenon	AE frequency (kHz)
Lubrication regime transitions [96, 105, 66]	50–200
Oil starvation of internal combustion engines [118]	20–30
Oil starvation [120]	100–300
Bearing wear [92]	15–30
Particle contamination [11]	100–700
Scratched bearing fault [95]	10–50
Eccentric bore bearing fault [96]	10–50
Rubbing [121]	25–70
Vapor cavitation [99]	175–570
Bearing wear (mixed friction) [104]	100–300
abnormal (postseizure) state [119]	1,500–2,000
Early seizure [119]	1,000
Later stage of adhesive wear [119]	300
Metal-to-metal contact (start) [119]	500
Metal-to-metal contact [105]	200–500

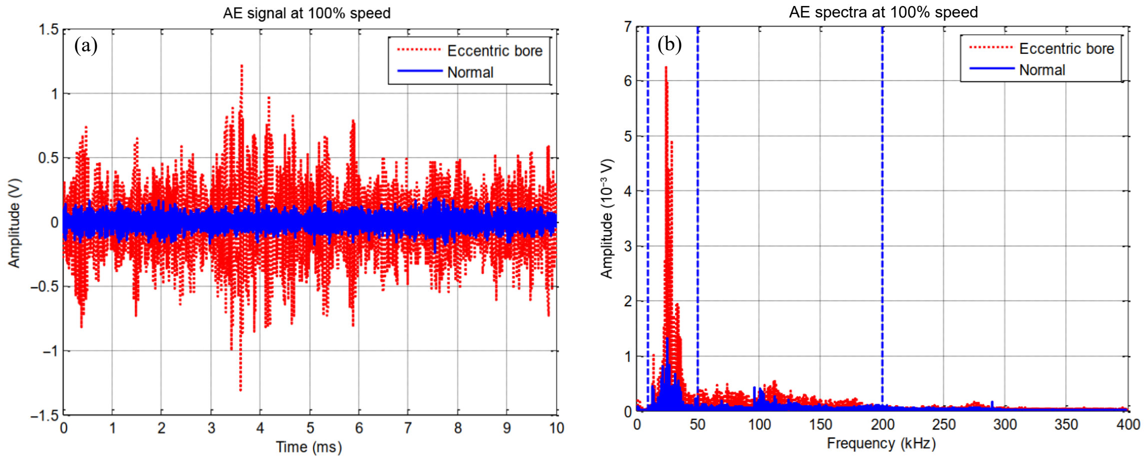

Fig. 13 Comparisons between normal and eccentric bore bearing faults: (a) AE signals; (b) AE spectra. Reproduced with permission from Ref. [96], © University of Huddersfield 2012.

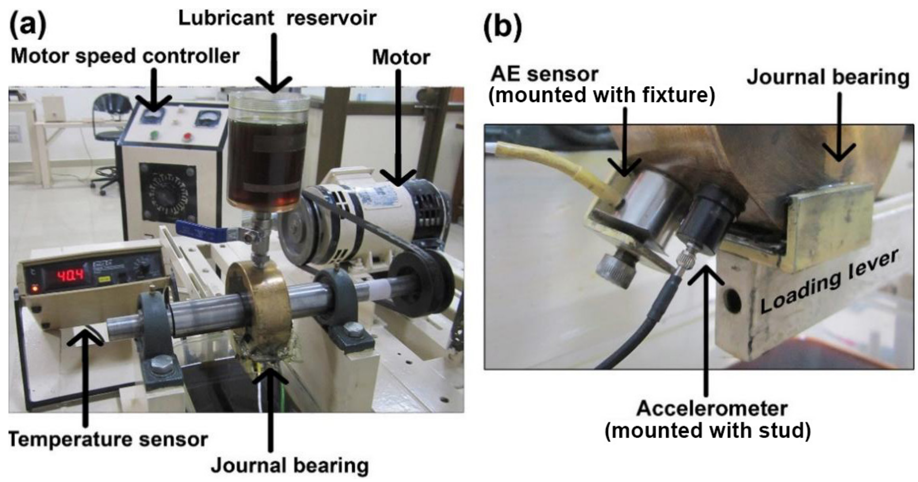

Fig. 14 (a) Journal bearing test rig; (b) location of AE sensor on journal bearing. Reproduced with permission from Ref. [11], © Elsevier Ltd. 2019.

frequency at 19 kHz. Renhart et al. [104] carried out repeated start–stop experiments to verify the degeneration of journal bearings and estimated a two-stage wear mechanism of journal bearings, which can be identified by the characteristic frequency of the AE signals, including the peak frequency and frequency band. Hase et al. [119] carried out friction-and-wear experiments on a journal bearing-rotor rig. They compared the distribution of the AE frequency obtained from the preseizure and postseizure of the journal bearing and found a peak frequency at 500 kHz in the normal state. Nevertheless, there was a peak frequency between 1,500 and 2,000 kHz for the abnormal state, as illustrated in Fig. 16. These results investigate the correlation between the AE frequency characteristics and the journal bearing behaviors, which can be directly used to monitor the condition and diagnose the faults of journal bearings.

3.2.3 Artificial intelligence methodology

Practically, the AE signals obtained from journal bearing tests are subject to significant noise contamination and experience attenuation of the AE energy during propagation. Traditional methods for accurately identifying the condition of journal bearings by extracting AE signal features have certain limitations. Therefore, applying artificial intelligence methods to analyze AE response to classify the different operating states of journal bearings has become an important research direction for achieving precise bearing condition identification. Researchers have employed artificial intelligence methods, such as support vector machines (SVMs), k-nearest neighbors (k-NNs), and artificial neural networks (ANNs), to classify the features of AE signals accurately [122]. These methods are also partially utilized in the fault monitoring of journal bearings.

The utilization of ANNs has become increasingly prevalent in recent years. The components of the ANN include the input layer, multiple neuron layers, one or more hidden layers, and the output layer. Sadegh et al. [123] employed continuous wavelet transform (CWT) techniques and time-domain analysis to extract AE features. They classified the lubricant conditions of journal bearings on the basis of the ANN combined with the genetic algorithm (GA). This method effectively identifies journal bearings operating under different lubrication regimes by accurately extracting AE features. If it is used to classify different bearing faults, further research on feature parameter extraction for each bearing fault is needed. The machine learning technique was employed by König et al. [124] to analyze AE signals obtained from heavy-load operating conditions at a low rotating speed. Using deep neural networks (DNNs), they successfully identified the different stages of bearing fatigue, such as running-in (mixed-friction) and particle contamination. CWTs of AE signals were utilized in this model as the input parameters, which significantly streamlined the efforts involved in feature extraction and analysis to detect and classify AE events. In addition, they monitored and classified the multivariate wear behavior of journal bearings by

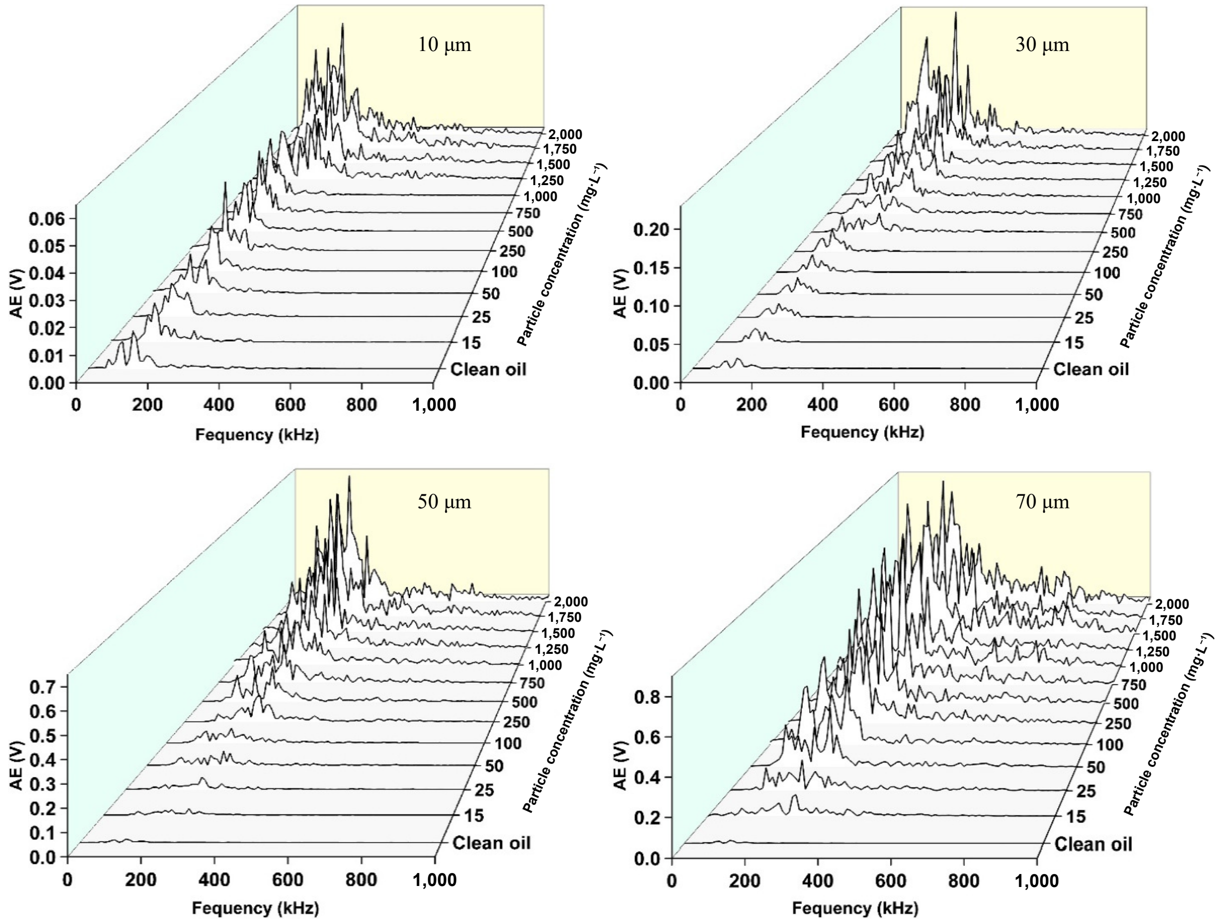

Fig. 15 AE spectra of journals bearing lubricant contaminants with different particle sizes. Reproduced with permission from Ref. [11], © Elsevier Ltd. 2019.

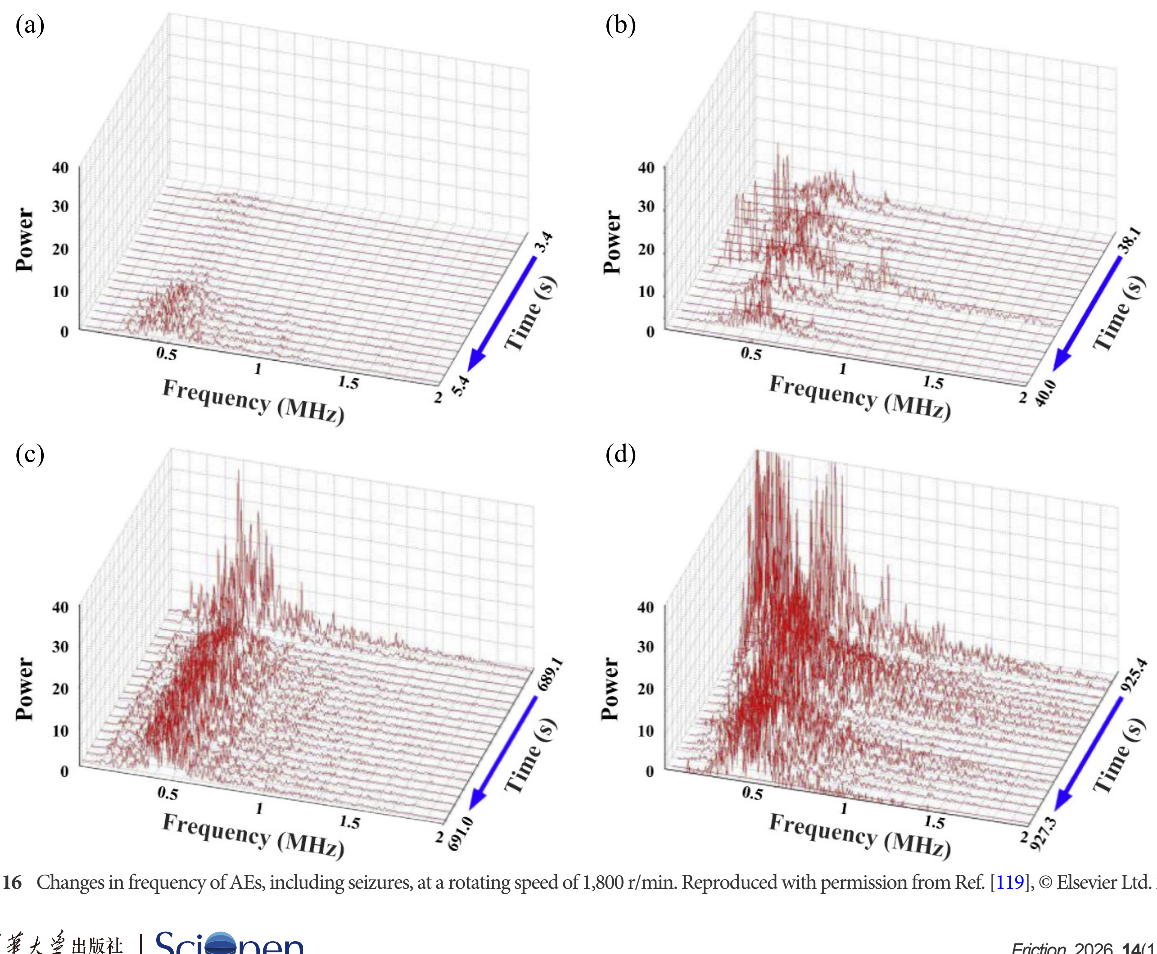

Fig. 16 Changes in frequency of AEs, including seizures, at a rotating speed of 1,800 r/min. Reproduced with permission from Ref. [119], © Elsevier Ltd. 2016.

applying a deep learning method combined with convolutional neural networks (CNNs) [125]. Subsequently, they monitored the mixed-friction conditions of journal bearings in gearboxes [126]; the topography of the worn surface is displayed in Fig. 17, and on the basis of long short-term memory (LSTM) neural networks, the wear volume of bearings can be predicted, as shown in Fig. 18. The k-NN algorithm determines the class or label of test data by calculating the distances between the test data and training data with known classes. Therefore, selecting the optimal value for k and defining the distance are crucial factors in this method. Poddar and Tandon [65] employed the peak frequency of AE signals as a condition indicator in various k-NNs for fault classification: the fine, medium, coarse, cosine, cubic, and weighted types. On the basis of the recognition accuracy analysis, they selected the weighted k-NN classifier combined with the Euclidean distance to successfully identify the conditions of journal bearings encompassing regular operation, cavitation, particle contamination, and oil starvation. Mokhtari and Gühmann [127] conducted journal bearing tests under various operating conditions and classified three different friction states: mixed, mild, and fluid. The states were determined using a linear SVM classifier, and the AE RMS and kurtosis were incorporated as training parameters to compute the significant frequency band obtained through the CWT.

To increase the accuracy of pattern recognition, AE signal processing and feature extraction play critical roles in these methodologies. The popular methods in the time–frequency domain for processing raw AE signals before feature extraction include the CWT, WT scalogram, reassigned wavelet scalogram, complex Morlet wavelet, and Wigner–Ville distributions. For bursting AE signals, the cyclostationary technique has advantages over traditional methods for signal processing. The AE feature focuses primarily on extracting the characteristics of the AE signals in both the time domain and the frequency domain, as introduced in Sections 3.2.1 and 3.2.2. In addition, some special calculated values can also be utilized as feature parameters, such as the correlation coefficient, coefficient of friction, Euclidean distance, and Mahalanobis distance. Research on the application of artificial intelligence algorithms to the condition monitoring of journal bearings is summarized in Table 4, which is categorized into three main areas: signal processing, feature extraction, and pattern recognition.

According to previous studies, the features extracted from AE signals can be used to identify the condition of journal bearings under controlled operating conditions. Practically, describing the internal mechanisms precisely through the aforementioned experimental studies is challenging. One reason is that the AE signals are obtained from journal bearings combined with other sources, especially when multiple faults occur at the same time. Furthermore, factors such as sensor placement and environmental background inevitably influence the AE signals, particularly with respect to the interference generated during signal propagation from the AE sources to the AE sensor. In addition, it is difficult to tightly control the test conditions to ensure the discussion of individual variables.

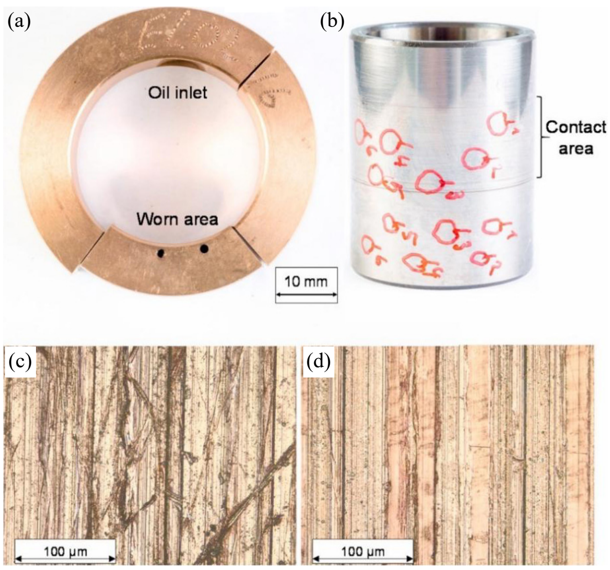

Fig. 17 Wear results: (a) worn bearing; (b) worn shaft sleeve specimen and positions for LSM analysis; (c) bearing surface without load; (d) bearing surface in loaded area (running-in type A). Reproduced with permission from Ref. [126], © Elsevier Ltd. 2021.

4 Modeling of AE

The research discussed above predominantly employs experimental methods to analyze the behavior of journal bearings

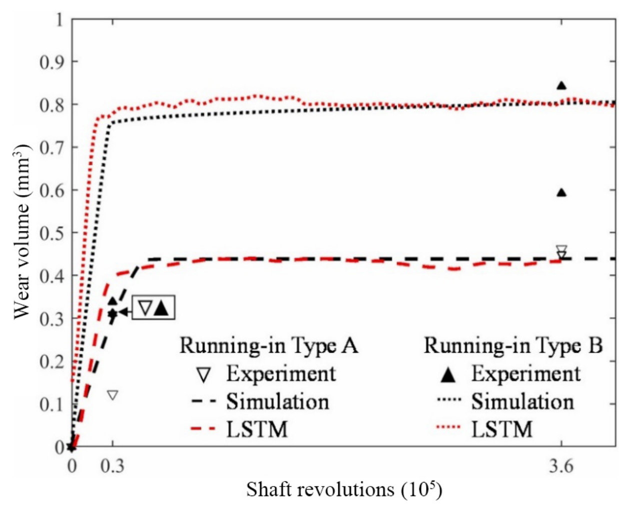

Fig. 18 Comparison of results from experiments, simulations, and LSTM for running-in conditions. Reproduced with permission from Ref. [126], © Elsevier Ltd. 2021.

Table 4 Methods of condition monitoring and fault diagnosis of journal bearings for AE signals

Signal processing	Feature extraction	Pattern recognition
Wavelet transform [121]		
Wavelet reassigned scalogram [121]	RMS, Kurtosis [123, 127]	ANN–GA [123]
Short-time Fourier transformation [60, 70]	Peak frequency [120, 123]	DNN [124]
CWT [103–105, 125]	Euclidean distance [65]	CNN [125]
Wigner–Ville distribution [128]	Mahalanobis distance [132]	Weighted k-NN [65]
Complex Morlet wavelet [129]	Correlation coefficient [132]	SVM [103, 127]
Cyclostationary [130]	Coefficient of friction [62]	LSTM [126]
Peak-hold-downsample algorithm [131]		

on the basis of AE signals. To further elucidate the mechanisms behind AE signal generation in journal bearings, numerous researchers have simultaneously focused on developing pertinent models of AE signals. Specifically, for the early-stage detection of lubrication surface faults in rotating machinery, much of the research has concentrated on constructing models that describe the AE signals generated by the elastic deformation of sliding friction pairs or microconvex asperities on rough surfaces. According to plate wave theory, the model acoustic emission (MAE) theory can be applied to analyze the AE phenomenon, which explains why AE is mechanical and propagates through plates as mechanical waves [121].

4.1 AE RMS model in the abrasive wear process

Matsuoka et al. [133] estimated the energy released by AE resulting from material removal in direct contact with solid surfaces in relative motion. According to Archard's equation, the wear coefficient is defined by Eq. (1):

$$k=\frac{VH}{WS} \tag{1}$$

where V represents the volume of material lost during the abrasion process, W denotes the external load, and H and S represent the hardness of the sample and the distance between the tape and the sample, respectively.

When the volume of material removed is V, the required energy can be calculated by Eq. (2):

$$W_t=VH \tag{2}$$

The material removal power is then derived from Eq. (3):

$$\dot{W}_\mathrm{r}=\frac{\mathrm{d}W_\mathrm{r}}{\mathrm{d}t}=\frac{\mathrm{d}(kWS)}{\mathrm{d}t}=kWv \tag{3}$$

where v is the speed of the relative sliding. The expression of the AE RMS can be derived from Eq. (4) on the basis of the correlation between the material removal power and the measured voltage of the AE signals:

$$V_\mathrm{RMS}=(ZkWv)^{1/2}+\varepsilon \tag{4}$$

where Z is the impedance of the measurement system and 6 is the "noise" in this system.

According to the AE RMS model, a correlation between the AE power and material removal power is established. Importantly, the state of wear can be estimated via the wear coefficient without measuring the volume of removed materials.

4.2 Model of AE energy, amplitude and count rate under sliding friction

After considering the influence of surface roughness, as illustrated in Fig. 19, Baranov et al. [54] proposed a model based on random function deviation theory to determine the AE parameters of solid contact friction in the sliding friction process. They described the fundamental characteristics of AE elastic waves and established the corresponding relationship between surface material parameters and AE generated by contact frictions.

The energy of the elastic deformation resulting from the contact between asperities is first determined by Eq. (5):

$$U_\mathrm{E}=\frac{8}{15M\sqrt{B}}h^5 \tag{5}$$

where M denotes the Hertzian contact modulus; as the contacted asperities are spherical shapes with radii R_1 and R_2, and the coefficient B is obtained as $B = (1 + R_1/R_2)/R_1$. Depending on the relationship between the average pressure p and the asperity radius a, h can be calculated by Eq. (6):

$$h=\left(\frac{9\pi^2}{16}\cdot M^2Bp^2a^4\right)^{1/2} \tag{6}$$

Substituting Eq. (6) into Eq. (5), the model of the AE energy is derived from Eq. (7):

$$U_\mathrm{E}=\frac{81\pi^5M^4}{640B^3}p^5 \tag{7}$$

Then, the amplitude of the AE signals is evaluated by Eq. (8):

$$A=K_0\left(\frac{v}{v_0}\right)^{\frac{1}{2}}\frac{p^2}{p_0^2} \tag{8}$$

where $K_0=[(3\pi^2K_c\sigma_1^2Rv_0)/(80M)]^{1/2}$, $p_0=(2B\sigma_1/3\pi)^{1/2}/M$, $v_0=1$ m/s; σ_1, v, K_c, and R represent the standard deviation of random functions $z_1(x)$ from corresponding average planes, the velocity of sliding motion of surfaces, an electromechanical conversion factor of a piezoelectric transducer, and the curvature radii of contacting asperities, respectively.

Consequently, depending on the distance d between the average planes of the surfaces, the average number of contact zones is N, and per nominal square L^2 of interaction, the count rate of the AE pulses can be derived from Eq. (9):

$$\frac{\mathrm{d}N}{\mathrm{d}t}=\frac{L\sigma^2v}{4\pi^2\sigma_1^2\eta}\exp\left(-\frac{d^2}{2\sigma_1^2\eta}\right) \tag{9}$$

where $\eta=1+\alpha^2$, with α being the ratio of the standard deviations of random functionsz_1 (x) and $z_2(x)$, as illustrated in Fig. 19. Assuming that $d/\sigma_1\sqrt{\eta}\approx\sqrt{f}$ and $f=-\ln(F/F_0)$, the count rate of the AE can be defined by Eq. (10):

$$\dot{N}_\mathrm{AE}=N_0\frac{L\sigma^2}{8\pi^2\sigma_1^2\eta}\frac{F_\mathrm{tot}}{F_0}v \tag{10}$$

where N_0 is an empirical coefficient that quantifies the number of AE pulses observed when a single contact zone is present; F_{tot} and F_0 represents the force pressing the surfaces together and the calculation coefficient with a force dimension.

The fundamental characteristics of AE elastic waves are described on the basis of the AE energy, amplitude, and count rate. Furthermore, a corresponding relationship between the surface material parameters and the AE generated by contact friction can be established. These models establish the dependence relationship between AE signals and the physical-mechanical properties of materials, as well as the statistical parameters of friction surface pairs. Notably, this research introduces the concept that the elastic energy released from the deformation of surface asperities is a primary AE source, representing a significant advancement in understanding AE origins in contact friction contexts.

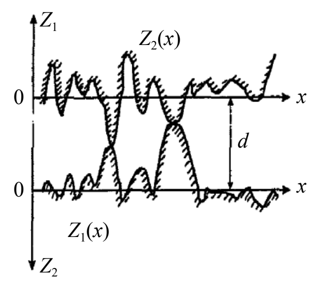

Fig. 19 Profiles of rubbing surfaces. Reproduced with permission from Ref. [54], © Elsevier Ltd. 1997.

4.3 Fan's statistical AE RMS model

The summit height of rough surfaces is assumed to follow a Gaussian distribution. Fan et al. [73] established an AE RMS theoretical model for the contact of asperities in the elastic sliding process on the basis of the Greenwood–Williamson (GW) model and Hertz elastic contact theory. In this model, the total energy stored in the elastic deformation of asperities can be calculated by Eq. (11):

$$U_{\mathrm{E}}=0.4A_{\mathrm{o}}D_{\mathrm{SUM}}W\int_{d}^{\infty}(z_{\mathrm{s}}-\mathrm{d})f(z_{\mathrm{s}})dz_{\mathrm{s}} \tag{11}$$

where the random variable z_s represents the height of the asperities on the rough surface; $f(z_s)$ is the probability density function of z_s; d is the distance between the smooth surface and the reference plane, as shown in Fig. 20; D_{sum} represents the total number of asperities per unit area; A_0 represents the contact area; W represents the normal load.

The function $F_n(h)$ and the number N_{tot} of contacting asperities are identified by Eqs. (12) and (13):

$$F_{\mathrm{n}}(h)=\int_{t}^{\infty}(s-h)^{n}\phi(s)\mathrm{d}s \tag{12}$$

$$N_{\mathrm{tot}}=A_{0}D_{\mathrm{SUM}}\int_{d}^{\infty}f(z_{\mathrm{s}})\mathrm{d}z_{\mathrm{s}} \tag{13}$$

where $h=d/\sigma$, with σ being the standard deviation of z_s; $\varphi(s)$ represents the standardized height distribution. Here, the mean time of the elastic energy release is given by Eq. (14):

$$\overline{\tau}=\frac{\int_{d}^{\infty}R'^{1/2}\delta^{1/2}f(z_{\mathrm{s}})dz_{\mathrm{s}}}{v\int_{\mathrm{d}}^{\infty}f(z_{\mathrm{s}})\mathrm{d}z_{\mathrm{s}}}=\frac{\int_{\mathrm{d}}^{\infty}R'^{1/2}(z_{\mathrm{s}}-\mathrm{d})^{1/2}f(z_{\mathrm{s}})dz_{\mathrm{s}}}{v\int_{d}^{\infty}f(z_{\mathrm{s}})dz_{\mathrm{s}}} \tag{14}$$

where $\delta=z_s-d$; v is the sliding velocity of the surface; R' represents the Hertzian curvature.

According to Eqs. (11) and (14), the energy rate of the AE

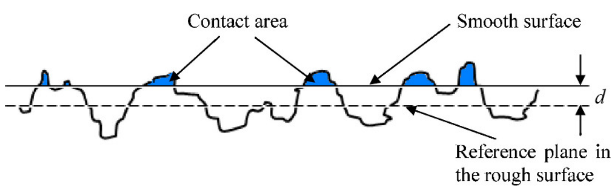

Fig. 20 Schematic of contact state between smooth and rough surfaces. Reproduced with permission from Ref. [73], © Elsevier Ltd. 2010.

generated from the elastic deformation of the contacted asperities is given by Eq. (15):

$$\dot{U}_{\mathrm{E}}=\frac{U_{\mathrm{E}}}{\overline{\tau}}=0.4NWv\frac{F_{1}(h)}{R'^{1/2}F_{1/2}(h)} \tag{15}$$

For the AE signals obtained by the AE sensor, the release rate of elastic energy can be derived from Eq. (16):

$$\dot{U}_{\mathrm{E}}=0.4k_{\mathrm{e}}k_{\mathrm{m}}N_{\mathrm{tot}}Wv\frac{F_{1}(h)}{R'^{1/2}F_{1/2}(h)} \tag{16}$$

where k_e is the portion of the elastic strain energy converted to acoustic emission pulses and k_m represents the gain of the AE measurement system.

As the velocity of the relative sliding surfaces is stable, $\dot{U}_A$ will be constant. Then, the RMS of the AE signals can be described by Eq. (17):

$$V_{\mathrm{rms}}=\sqrt{\dot{U}_{\mathrm{E}}}=\left(\frac{2k_{\mathrm{e}}k_{\mathrm{m}}}{5}\right)^{1/2}N_{\mathrm{tot}}{}^{1/2}(Wv)^{1/2}\frac{F_{1}(h)^{1/2}}{R'^{1/4}F_{1/2}(h)^{1/2}} \tag{17}$$

In the above model, the relationships between the level of the AE measurement and the sliding speed, the characteristics of the rough surfaces, the load, and the number of contacting asperities on the rough surface are described clearly. The reliability of the model was further validated by monitoring the operating conditions of mechanical seals via experimental investigations. Importantly, this model demonstrates significant potential for the early detection and evaluation of premature mechanical failure.

Subsequently, Hu et al. [64, 134] proposed a deterministic AE RMS model for a sliding surface characterized by a bi-Gaussian distribution in terms of topography, as shown in Fig. 21(a). Merging model parameters, Fan's model is derived from Eq. (18):

$$\mathrm{RMS}_{\mathrm{avg}}=K\left(\frac{2}{5}EvD_{\mathrm{s}}\int_{h_0}^{\infty}\delta^{2}\mathrm{PDF}(z_{\mathrm{s}})\,\mathrm{d}z_{\mathrm{s}}\right)^{1/2} \tag{18}$$

where $\delta=z_s-d$, with z_s and d being the height of the asperities and the distance between the smooth surface and the plane at the mean height of the rough surface, respectively; K, E, and D_s represent the constant transfer coefficient, which is equivalent to Yong's modulus, and the density of asperities.

The load acting on the asperities when the height exceeds h_0 is calculated by Eq. (19):

$$W=(z_{\mathrm{s}}-d)^{3/2}ER_{\mathrm{s}}^{1/2} \tag{19}$$

As the friction pair is within the elastic deformation range, only the summit on the upper component has the potential to be the

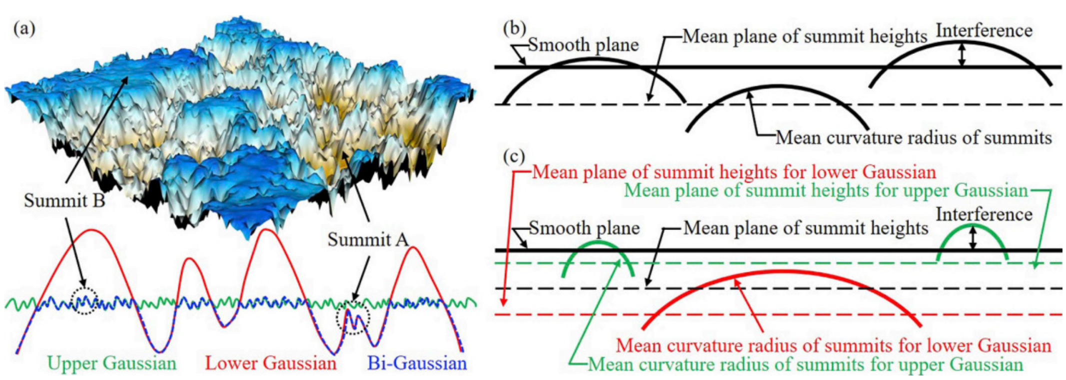

Fig. 21 AE RMS model under dry sliding friction: (a) bi-Gaussian stratified surface; (b) Fan's statistical AE RMS model; (c) statistical AE RMS model from a bi-Gaussian stratified surface. Reproduced with permission from Ref. [64], © Elsevier Ltd. 2019.

AE source. Therefore, the rough surfaces shown in Fig. 21(b) should be replaced by the bi-Gaussian stratified surface described in Fig. 21(c) to exclude interference due to the summit on the lower component. For these contacting rough surfaces, the equivalent radius of curvature R_s can be expressed as Eqs. (20) and (21) [135, 136]:

$$R_s = \frac{1}{1/R_{sx} + 1/R_{sy}} \tag{20}$$

$$R_{sx} = \frac{\Delta_x^2}{2z_{si,j} - z_{si,j-1} - z_{si,j+1}}, R_{sy} = \frac{\Delta_y^2}{2z_{si,j} - z_{si-1,j} - z_{si+1,j}} \tag{21}$$

where R_{sx} and R_{sy} are the curvature radii; Δ_x and Δ_y are the sampling intervals, with the subscripts x and y denoting the directions.

Practically, a bi-Gaussian surface topography is more consistent with the characteristics of the sliding friction surfaces. The AE RMSs generated from different materials were calculated on the basis of the deterministic AE RMSs and Fan's models. Moreover, the AE RMS is highly sensitive to the parameters of the surface.

4.4 AE RMS model of fractal rough surfaces under sliding friction

Owing to the plastic deformation disregarded in the process of friction contacts based on the G–W model, the Majumdar–Bhushan (M–B) model is then employed to describe this phenomenon. Hao et al. [137] revised the M–B model combined with fractal rough surfaces. The updated model eliminates the assumption of total elastic deformation and incorporates three distinct states: elastic, elastic–plastic, and plastic. The critical value of asperity deformation at the beginning of plastic flow is proportional to the square of the material hardness H and the radius of curvature r and inversely proportional to the square of the Young's modulus E, as noted by Greenwood and Williamson [138]. Therefore, the criterion for evaluating the deformation ratio is given by Eq. (22):

$$\eta_c = \frac{\delta_c}{r} = b\left(\frac{H}{E}\right)^2 \tag{22}$$

For the G–W model, the critical interference is expressed as Eq. (23):

$$\delta_c^{GW} = r\eta_c \tag{23}$$

According to Eq. (23), if the amplitude of the asperity is $\delta < \delta_c^{GW}$ $(\delta = G^{(D-1)} l^{(2-D)})$, the deformation of the asperity is elastic; conversely, the deformation is plastic. For the M–B model, the critical interference is defined by Eq. (24):

$$\delta_c = \frac{G}{M^{(2-D)/2(D-1)}} \tag{24}$$

where $M = \eta_c/(2\pi)^2$; G denotes a parameter of the surface's fractal roughness, indicating its characteristic length scale; D is the fractal dimension for a physically continuous surface ($1 < D < 2$).

Herein, the elastic deformation occurs at $\delta > \delta_c$, and the plastic deformation occurs at $\delta \leq \delta_c$. On the basis of Eq. (24), the critical value δ_c is independent of the characteristics of the asperities. The total energy generated by the asperity's deformation in sliding friction can be described by Eq. (25):

$$\begin{aligned} U_{sum} &= \int_0^{\delta_l} P(\delta) n(\delta) \delta \mathrm{d}\delta \\ &= \begin{cases} \int_0^{\delta_l} P_p(\delta) n(\delta) \delta \mathrm{d}\delta, & \delta_l \leq \delta_c \\ \int_0^{\delta_c} P_p(\delta) n(\delta) \delta \mathrm{d}\delta + \int_{\delta_c}^{\delta_l} P_e(\delta) n(\delta) \delta \mathrm{d}\delta, & \delta_l > \delta_c \end{cases} \end{aligned} \tag{25}$$

The expressions of the plastic load and the elastic load can be given by Eq. (26):

$$P_p(\delta) = H\frac{\delta^{2/(2-D)}}{G^{2(D-1)/(2-D)}}, P_e(\delta) = \frac{4}{3}Er^{1/2}\delta^{3/2} = \frac{2E\delta^{(3-D)/(2-D)}}{3\pi G^{(D-1)/(2-D)}} \tag{26}$$

where $n(\delta) = \frac{D}{2-D}\frac{\delta_l^{D/(2-D)}}{\delta^{2/(2-D)}}$. The largest interference δ_l can be given by Eq. (27):

$$\delta_l = JF_N^{(2-D)/(3-D)} \tag{27}$$

where $J = \left[\frac{3\pi(2-D)}{2ED}\right]^{(2-D)/(3-D)} G^{(D-1)/(3-D)}$ and F_N is the normal load. By substituting Eqs. (26) and (27) into Eq. (25), the energy release rate is derived from Eq. (28):

$$\dot{U}_{sum} = \frac{U_{sum}}{T} = \begin{cases} \frac{vHD}{2\pi R_s(2-D)G^{2(D-1)/(2-D)}} J^{2/(2-D)} F_N^{2/(3-D)}, \\ \delta_l \leq \delta_c \\ \frac{v}{2\pi R_s}\left[\left(\frac{5H\delta_c}{G^4} - \frac{10E\ln\delta_c}{3\pi G^2}\right) J^5 F_N^{5/4} \right. \\ \left. + \frac{10EJ^5F_N^{5/4}\ln\left(JF_N^{1/4}\right)}{3\pi G^2}\right], \delta_l > \delta_c, D = 5/3 \end{cases} \tag{28}$$

where v is the sliding velocity and R_s represents the radius of the inside surface of the seal.

During the stable sliding friction process, the RMS of the AE signals acquired by the AE sensor in the AE measurement system can be calculated by Eq. (29):

$$V_{RMS} = \sqrt{k_e k_m \dot{U}_{sum}} \tag{29}$$

Unlike Fan's model, the fractal AE model can be used to characterize the elastic and plastic deformations of asperities on rough surfaces, which are influenced by factors such as the sliding velocity, normal load, and fractal parameters.

4.5 Fluid-asperity shearing model

The generation mechanism of AEs and the corresponding AE models have been extensively investigated in HL regimes for various applications, including internal combustion engines, mechanical seals, and journal bearings.

On the basis of Fan's model, Towsyfyan et al. [70, 139] developed an AE model of asperity elastic deformation by considering that every asperity was an end-loaded cantilever beam and discussed the AE energy statistics of the mechanical seal surfaces working in different lubrication states. The AE source was analyzed during the bending deformation of asperities, including interactions between asperities and fluid–asperity. The progress of energy release from the contact between asperities is illustrated in Fig. 22. The total strain energy is described by Eqs. (30) and (31):

$$U_{\mathrm{E(a\text{-}a)}} = A_0 D_{\mathrm{SUM}} \frac{f W^2}{6EI} \int_d^{\infty} (z_s - \mathrm{d})^3 f(z_s)\mathrm{d}z_s \tag{30}$$

$$U_{\mathrm{E(f\text{-}a)}} = A_0 D_{\mathrm{SUM}} \frac{(\mu \pi v r^2)^2}{6EI} \int_d^{\infty} (z_s - d) f(z_s)\mathrm{d}z_s \tag{31}$$

where $\delta = z_s - d$; f represents the friction coefficient; I is the area moment of inertia; μ represents the viscosity of the lubricant.

The equations used to calculate the mean release time are derived from Eqs. (32) and (33):

$$\bar{t}_{\mathrm{a\text{-}a}} = \frac{2f\sqrt{r}\int_d^{\infty} (z_s - \mathrm{d})^{\frac{9}{2}} f(z_s)\mathrm{d}z_s}{3Iv\int_d^{\infty} f(z_s)\mathrm{d}z_s} \tag{32}$$

$$\bar{t}_{\mathrm{f\text{-}a}} = \frac{2\mu\pi r^2\int_{\mathrm{d}}^{\infty} (z_s - \mathrm{d})^2 f(z_s)\mathrm{d}z_s}{3EI\int_d^{\infty} f(z_s)\mathrm{d}z_s} \tag{33}$$

where E and r are the equivalent elastic modulus and average radius of an asperity, respectively, given by Hertz theory. For the AE measurement system, the AE RMS of signals generated from the asperities bending in the sliding friction can be expressed by Eqs. (34) and (35):

$$V_{\mathrm{RMS(a\text{-}a)}} = \frac{W}{2r^{\frac{1}{4}}}\sqrt{k_e k_m \frac{f N_{\mathrm{tot}} v F_3(d*)}{E F_{\frac{9}{2}}(d*)}} \tag{34}$$

$$V_{\mathrm{RMS(f\text{-}a)}} = \frac{vr}{2}\sqrt{k_e k_m \mu \pi N_{\mathrm{tot}} \frac{F_1(d*)}{F_2(d*)}} \tag{35}$$

where $N_{\mathrm{tot}} = A_0 D_{\mathrm{SUM}} \int_d^{\infty} f(z)\mathrm{d}z$; $d* = d/R_q$; R_q is the equivalent roughness.

Depending on the shear stress τ_{zx} acting on any arbitrary stress in the sliding direction, as shown in Fig. 23, the viscosity friction force is calculated by Eq. (36)

$$\mathrm{d}F = \tau_{zx}\mathrm{d}A \tag{36}$$

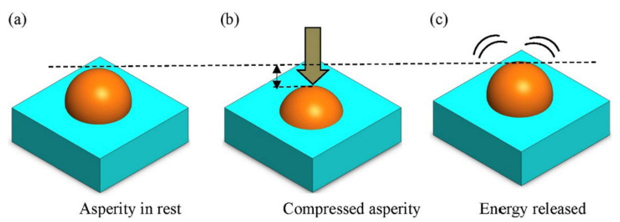

Fig. 22 Process of strain energy release during sliding contact. Reproduced with permission from Ref. [139], © Elsevier Ltd. 2018.

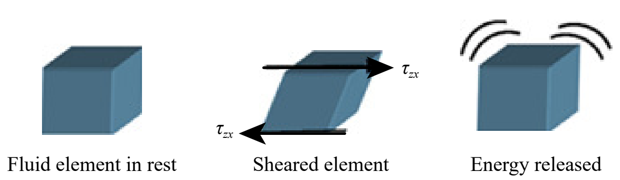

Fig. 23 Process of strain energy release due to viscous friction. Reproduced with permission from Ref. [139], © Elsevier Ltd. 2018.

The release rate of energy caused by viscosity friction can be defined by Eq. (37):

$$\dot{U}_{\mathrm{E}} = k_e k_m \iint v\mathrm{d}F = 2\pi k_e k_m \mu \frac{v^2}{h_f} r_m b \tag{37}$$

where h_f is the lubricant film thickness and r_m denotes the mean radius for the seal area. As the constant parameters in Eq. (35) are replaced by $K = \sqrt{2\pi k_e k_m b r_m}$, the viscosity friction model is expressed as Eq. (38):

$$V_{\mathrm{RMS}} = \sqrt{\dot{U}_{\mathrm{E}}} = Kv\sqrt{\frac{\mu}{h_f}} \tag{38}$$

The developed models have focused primarily on the bending deformation of the contacting asperities. In addition, Wei et al. [71] studied the effectiveness of applying the asperity–asperity collision model in internal combustion engines and proposed the concept of fluid–asperity shearing in the HL regime.

Ma et al. [55, 140] analyzed the AE generated from journal bearings due to the interaction between fluid and asperities in the HL regime, as shown in Fig. 24. The progress of fluid–asperity shearing was investigated in Fig. 6(c), and the dynamic FAS model was derived on the basis of the stationary Reynolds equation combined with a nonGaussian rough surface. In the model, the average friction force F due to fluid shearing is calculated by Eq. (39):

$$F = \iint \tau(x,y)\mathrm{d}x\mathrm{d}y \tag{39}$$

where the shear stress $\tau(x,y) = \mu(T)\dot{\gamma}(x,y) = \mu(T)\partial v/\partial z$, with the lubricant viscosity $\mu(T) = \mu_0 \mathrm{e}^{-\beta(T-T_0)}$, with μ_0 denoting the dynamic viscosity when the temperature is T_0 and β denoting the coefficient of temperature. For laminar flow, the velocity gradient v in the z direction is given by Eq. (40):

$$\frac{\partial v}{\partial z} = \frac{\partial v}{\partial h} + \frac{\partial p}{\partial x}\frac{1}{\mu(T)}\left(z - \frac{h_f}{2}\right) \tag{40}$$

The friction force is expressed as Eq. (41):

$$F = \iint \left(\mu_0 \mathrm{e}^{-\beta(T-T_0)}\frac{\pm v}{h_f} \pm \frac{h_f}{2}\frac{\partial p}{\partial x}\right)\mathrm{d}x\mathrm{d}y \tag{41}$$

where the oil film thickness h_f is a sum of the nominal height h_0 and the time-varying height $\delta_{\mathrm{asp}}(x,y,t)$ in the HL regime. According to Eq. (41), the average friction force F remains constant in the steady lubrication process. Therefore, the dynamic AE waves or the spectral characteristics of AEs are difficult to explain, depending on the model. Moreover, in terms of the reasons for the generation of AE waves, the distribution of asperities is the primary cause in fluid-separated plates. The pressure p is contributed mainly by the p_{asp} obtained from the rough surface. The dynamic fluid–asperity shearing in the HL can be defined by Eq. (42):

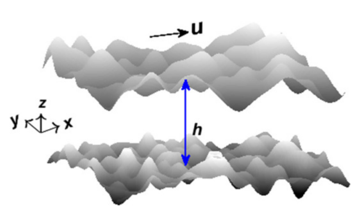

Fig. 24 Schematic diagram of relatively sliding rough surfaces in HL regime. Reproduced with permission from Ref. [55], © Elsevier Ltd. 2021.

$$\tau_{asp}(x,y,t)=\mu_0 e^{-\beta(T-T_0)}\frac{\pm v}{h_0+\delta_{asp}(x,y,t)}\pm\frac{h_0+\delta_{asp}(x,y,t)}{2}\frac{\partial p_{asp}}{\partial x} \tag{42}$$

According to Eq. (42), the dynamic FAS results from the viscous drag and pressure gradient in the x direction. Moreover, the time-varying nature of the force is due to the varying heights of asperities on the sliding surfaces. In addition to roughness, nonGaussian properties such as skewness and kurtosis need to be considered when building rough surfaces. To verify the influence of asperity distributions on the dynamic FAS, generating a random rough surface is a critical step. Then, the time-varying height of the rough surface is given by Eq. (43):

$$\delta_{asp}(r,\theta,t)=\sum z_i \sin\left(2\pi r\chi_i(\theta+\Omega t)+\zeta_i\right) \tag{43}$$

where $z_i=\sqrt{2Q\left(\chi_{mid,i}\right)\Delta\chi_i}$, χ_i, $\chi_{mid,i}$, and $\Delta\chi_i$ represent the spatial frequency, center frequency, and width of each frequency interval, respectively, r, Ω, Q, and ζ_i denote the ratio of the rotating surface, angular speed, spatial power spectral density (PSD) at random heights, and random initial phase angles, respectively.

In the context of the dynamic FAS model, the influence of various parameters, including the lubricant viscosity, sliding speed, oil film thickness, and pressure gradient, on the intensity of AE waves is evident. Additionally, the relationships among the non-Gaussian surface parameters of the relative sliding surfaces, operating conditions, and AE waves are investigated in the frequency domain through numerical and experimental analyses. The findings, as depicted in Figs. 25 and 26, indicate that the correlation length (spatial PSD) and shear rate (rotational speed) are critical parameters affecting the AE spectral bandwidth. The proposed model provides an analytical expression for fluid–asperity interactions, enabling quantitative assessment of their dynamic interactions.

On the basis of the above analysis, the main AE models, which depend on the mechanism of the AE signals generated from the relative sliding surfaces, are described in Table 5, and the research on their application in journal bearings is summarized.

5 Discussion and outlooks

The application of the AE technique for condition monitoring and fault diagnosis of journal bearings remains relatively limited compared with its use with seals, gears, roller bearings, etc. However, as a nondestructive detection method, the AE technique offers distinct advantages for evaluating the condition of sliding surfaces, especially in the early detection of rotor machinery failures. Consequently, this technology has gained increasing attention for monitoring journal bearings in recent years. Although significant progress has been achieved, there is a need for further development to address existing gaps and explore new directions. Future research opportunities in this field are outlined as follows:

(1) Elucidating a deeper mechanism of AE sources for journal bearings' early faults. Currently, the fault detection in journal bearings using AE signals focuses primarily on sliding friction, such as abrasive and adhesive wear. However, the main advantage of the AE technique lies in its sensitivity to monitor the incipient stages of faults in journal bearings. Therefore, the underlying cause needs to be revealed in the mechanism analysis of AE sources, especially with respect to analyses related to the second type of AE source. In addition, the accuracy of the AE measurement system plays a significant role in acquiring reliable AE signals. Improving the measurement system is necessary to increase the signal-to-noise ratio, particularly for effectively capturing the weak signal amid complex interference noise.

(2) Advancing AE waveform analysis for early fault detection. With advancements in AE technology, increasingly comprehensive data on AE waveforms can be obtained. While certain bearing faults have been effectively detected using statistical parameters such as the AE RMS and AE energy in the time domain, limited research has focused on journal bearings on the basis of their specific AE waveforms, particularly in the context of aperiodic early faults. Consequently, extracting meaningful information from AE waveforms remains a significant challenge, as it has the potential to offer a more intuitive representation of initial faults in bearings.

(3) High-order spectral techniques for AE signal denoising.

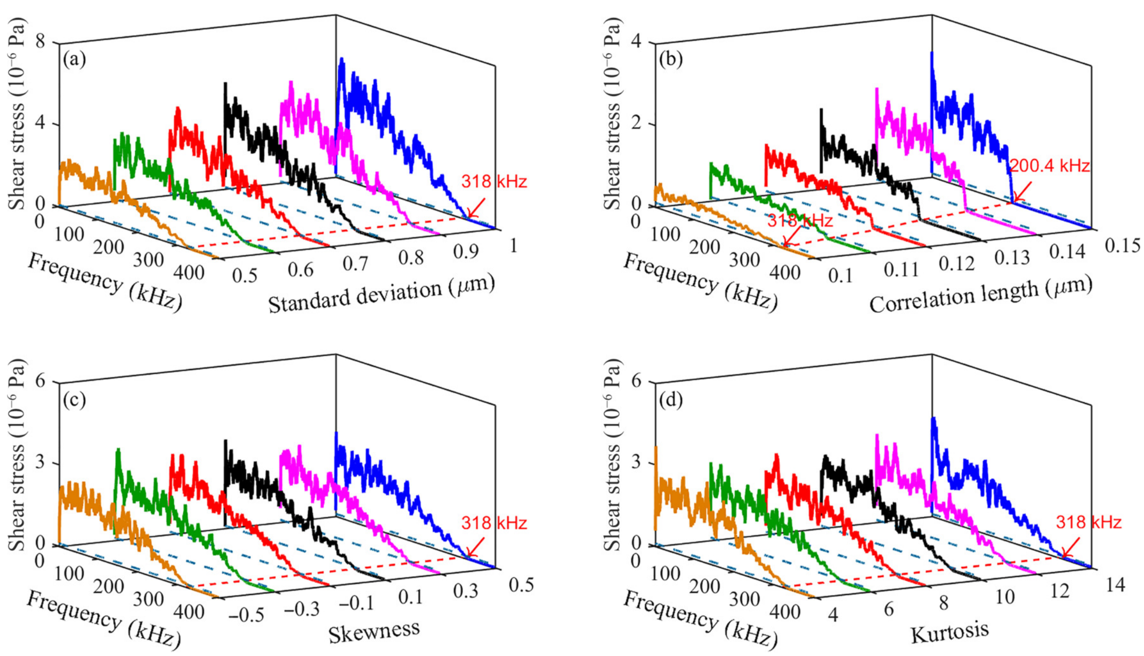

Fig. 25 Frequency spectra of FAS at a shear rate of 4,000 s^{-1} with different surface parameters. Reproduced with permission from Ref. [55], © Elsevier Ltd. 2021.

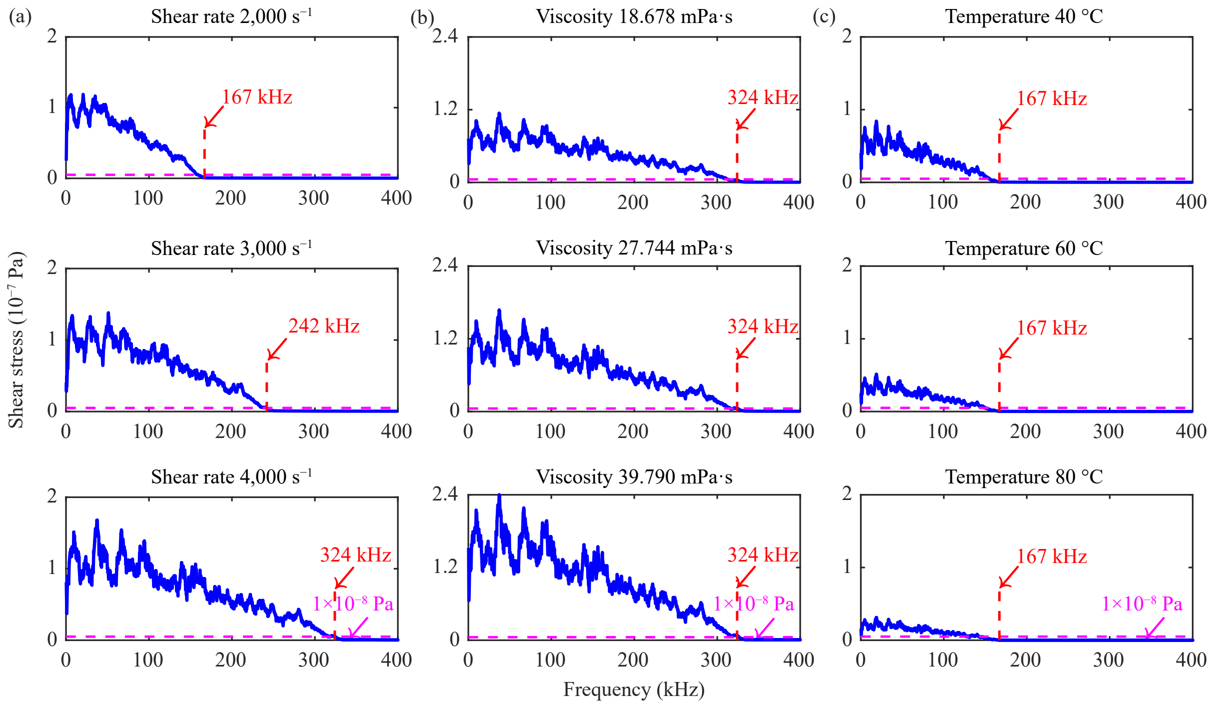

Fig. 26 Frequency spectra of FAS generated from the cone plate under various operating conditions. Reproduced with permission from Ref. [55], © Elsevier Ltd. 2021.

Table 5 AE model

Model	Equation	Ref.
AE RMS model (material removal in the abrasion process)	$V_{\mathrm{RMS}} = (ZkWv)^{1/2} + \varepsilon$	[133]
Model of AE energy, amplitude, and count rate (sliding friction)	$U_{\mathrm{E}} = \frac{81\pi^5 M^4}{640B^3}p^5$, $A = A_0\left(\frac{v}{v_0}\right)^{\frac{1}{2}}\frac{p^2}{p_0^2}$, $\dot{N}_{\mathrm{AE}} = N_0\frac{L\sigma^2}{8\pi^2\sigma_1^2\eta}\frac{F_{\mathrm{tot}}}{F_0}v$	[54]
Fan's AE RMS model (elastic sliding of asperities contact)	$V_{\mathrm{rms}} = \left(\frac{2k_{\mathrm{e}}k_{\mathrm{m}}}{5}\right)^{1/2} N_{\mathrm{tot}}{}^{1/2}(Wv)^{1/2}\frac{F_1(h)^{1/2}}{R'^{1/4}F_{1/2}(h)^{1/2}}$	[73, 96]
AE RMS model (bi-Gaussian rough surface; sliding friction)	$\mathrm{RMS}_{\mathrm{avg}} = K\left(\frac{2}{5}EvD_{\mathrm{s}}\int_{h_0}^{\infty}\delta^2\mathrm{PDF}(z_{\mathrm{s}})\,\mathrm{d}z_{\mathrm{s}}\right)^{1/2}$	[64, 134]
AE RMS model (fractal rough surfaces)	$V_{\mathrm{RMS}} = \sqrt{k_{\mathrm{e}}k_{\mathrm{m}}U_{\mathrm{sum}}}$	[137]
Viscosity friction model (full film condition)	$V_{\mathrm{RMS}} = Kv\sqrt{\frac{\mu}{h_{\mathrm{f}}}}$	[70, 139]
FAS model (full film condition; non-Gaussian rough surface)	$\tau_{\mathrm{asp}}(x,y,t) = \mu(T)\frac{\pm v}{h_{\mathrm{f}}(x,y,t)} \pm \frac{h_{\mathrm{f}}(x,y,t)}{2}\frac{\partial p_{\mathrm{asp}}}{\partial x}$	[55]

Traditional denoising techniques have been employed to process raw AE signals; however, their effectiveness in suppressing noise under field conditions remains limited. This limitation highlights the need to develop more advanced denoising methods specifically designed for field applications, considering that AE signals from journal bearings exhibit non-Gaussian and nonlinear characteristics. High-order spectral analysis offers a robust solution, as it is inherently resistant to Gaussian noise and effectively reduces its impact. Among these methods, bispectral analysis is particularly notable for its simplicity. It not only compensates for the absence of phase information in the power spectrum but also efficiently attenuates noise. Consequently, employing high-order spectral noise reduction techniques can significantly improve the accuracy of fault detection in AE signal analysis.

(4) Enhancing data fusion for intelligent identification methods. The existing research has confirmed the feasibility of using intelligent methods for fault identification in journal bearings on the basis of AE signals. However, the corresponding research is limited in this area and focuses primarily on identifying typical faults that occur during contact between relatively sliding surfaces. Furthermore, the intelligent identification methods employed, such as the CNN, ANN, and k-NN, have been relatively basic. Therefore, it is imperative to develop deep data fusion technologies to enhance decision-making capabilities by integrating multiple monitoring technologies.

(5) Establishing the failure database for journal bearings. Artificial intelligence techniques have demonstrated significant advantages in bearing fault identification. However, to achieve accurate fault monitoring, the training data must include corresponding fault information to establish a precise identification system. Therefore, the presence of sufficient fault-type data in the training set is necessary for the establishment of a bearing fault identification system. Since the acquired AE signals

are influenced by the monitoring system, standardizing the AE monitoring system becomes crucial for obtaining unified training data and establishing a comprehensive journal bearing fault recognition system. Selecting appropriate fault feature quantities and establishing a journal bearing fault database based on them will be an important focus for future research.

(6) Refining the AE model on the basis of mechanism analysis. At present, the existing AE models rely primarily on the energy release resulting from the relative sliding surfaces. Moreover, each model requires particular preconditions for its application. To comprehensively determine the states of journal bearings and accurately identify early faults, it is crucial to have an appropriate AE model. A comprehensive examination of current research endeavors revealed that initial failures in journal bearings can lead to subtle changes in both the lubrication medium and the relative sliding surfaces. Therefore, future research should correlate these two parameter variations and establish a more universally applicable AE model. For example, a model specifically targeting early oil contamination in journal bearings can be derived by refining the FAS model with fluid rheological properties.

6 Concluding remarks

The application of AE technology in the condition monitoring and fault diagnosis of journal bearings is analyzed and summarized by reviewing the latest processes in this field. The AE sources during various operational states of journal bearings are comprehensively introduced. The performance characteristics of AE waves are utilized to compare and analyze the signal processing methods commonly employed, along with their respective strengths and limitations, as evidenced by existing research results. The physical models commonly used to explain the generation mechanisms of AE waves are presented, and the specific conditions applicable to each model are summarized. According to the current research findings, the utilization of AE technology in journal bearings enables enhanced early fault monitoring capabilities. This review aims to analyze the current research on fault diagnosis of sliding bearings via AE technology to guide a more effective health assessment of sliding bearings, offering valuable insights to promote the widespread application of acoustic emission technologies in the condition monitoring of rotating lubricated machinery.

Acknowledgements

This research is supported by the National Natural Science Foundation of China (No. 52205089), the Guangdong Basic and Applied Basic Research Foundation (No. 2021A1515110767), and the Tribology Science Fund of the State Key Laboratory of Tribology in Advanced Equipment (No. SKLTKF22B15).

Declaration of competing interest

The authors have no competing interests to declare that are relevant to the content of this article.

References

[1] Miettinen J, Siekkinen V. Acoustic emission in monitoring sliding contact behaviour. *Wear* **181–183**: 897–900 (1995)

[2] Lindley C A, Beamish S, Dwyer-Joyce R S, Dervilis N, Worden K. A Bayesian approach for shaft centre localisation in journal bearings. *Mech Syst Signal Pr* **174**: 109021 (2022)

[3] Jia Y P, Dou P, Zheng P, Wu T H, Yang P P, Yu M, Reddyhoff T. High-accuracy ultrasonic method for *in situ* monitoring of oil film thickness in a thrust bearing. *Mech Syst Signal Pr* **180**: 109453 (2022)

[4] Jin Y Z, Chen F, Xu J M, Yuan X Y. Nonlinear dynamic analysis of low viscosity fluid-lubricated tilting-pad journal bearing for different design parameters. *Friction* **8**(5): 930–944 (2020)

[5] Yang Y, Tang J Y, Hu N Q, Shen G J, Li Y H, Zhang L. Research on the time-varying mesh stiffness method and dynamic analysis of cracked spur gear system considering the crack position. *J Sound Vib* **548**: 117505 (2023)

[6] Fu C, Sinou J J, Zhu W D, Lu K, Yang Y F. A state-of-the-art review on uncertainty analysis of rotor systems. *Mech Syst Signal Pr* **183**: 109619 (2023)

[7] Fu C, Zhu W D, Ma J J, Gu F S. Static and dynamic characteristics of journal bearings under uncertainty: A non-probabilistic perspective. *J Eng Gas Turb Power* **144**(7): 071012 (2022)

[8] Ning C X, Hu F, Ouyang W, Yan X P, Xu D L. Wear monitoring method of water-lubricated polymer thrust bearing based on ultrasonic reflection coefficient amplitude spectrum. *Friction* **11**(5): 685–703 (2023)

[9] Rho B H, Kim K W. Acoustical properties of hydrodynamic journal bearings. *Tribol Int* **36**(1): 61–66 (2003)

[10] Mokhtari N, Knoblich R, Nowoisky S, Bote-Garcia J L, Gühmann C. Differentiation of journal bearing friction states under varying oil viscosities based on acoustic emission signals. In: Proceedings of the IEEE International Conference on Prognostics and Health Management, 2019: 1–7.

[11] Poddar S, Tandon N. Detection of particle contamination in journal bearing using acoustic emission and vibration monitoring techniques. *Tribol Int* **134**: 154–164 (2019)

[12] Wan B, Yang J G, Sun S C. A method for monitoring lubrication conditions of journal bearings in a diesel engine based on contact potential. *Appl Sci* **10**(15): 5199 (2020)

[13] Pennacchi P, Vania A, Chatterton S. Nonlinear effects caused by coupling misalignment in rotors equipped with journal bearings. *Mech Syst Signal Pr* **30**: 306–322 (2012)

[14] Ma J J, Fu C, Zheng Z L, Lu K, Yang Y F. The effects of interval uncertainties on dynamic characteristics of a rotor system supported by oil-film bearings. *Lubricants* **10**(12): 354 (2022)

[15] Hamel M, Addali A, Mba D. Monitoring oil film regimes with acoustic emission. *P I Mech Eng J—J Eng* **228**(2): 223–231 (2014)

[16] Xue S, Howard I, Wang C S, Bao H, Lian P Y, Chen G G, Wang Y, Yan Y F. The diagnostic analysis of the planet bearing faults using the torsional vibration signal. *Mech Syst Signal Pr* **134**: 106304 (2019)

[17] Huang Q, Li L P, Rao H D, Jin F H, Tang Y Q. The AE law of sliding bearings in rotating machinery and its application in fault diagnosis. In: Proceedings of the International Conference on Power Engineering, 2007: 541–546.

[18] Ranjan R, Ghosh S K, Kumar M. Fault diagnosis of journal bearing in a hydropower plant using wear debris, vibration and temperature analysis: A case study. *P I Mech Eng E—J Pro* **234**(3): 235–242 (2020)

[19] Kasolang S, Ahmed D I, Dwyer-Joyce R S, Yousif B F. Performance analysis of journal bearings using ultrasonic reflection. *Tribol Int* **64**: 78–84 (2013)

[20] Beamish S, Li X, Brunskill H, Hunter A, Dwyer-Joyce R. Circumferential film thickness measurement in journal bearings via the ultrasonic technique. *Tribol Int* **148**: 106295 (2020)

[21] Koetz F, Schmitt F, Kirchner E, Zancul E. Visualising the lubrication condition in hydrodynamic journal bearings using impedance measurement. *Front Mech Eng* **10**: 1456575 (2024)

[22] Pomponi E, Vinogradov A. A real-time approach to acoustic emission clustering. *Mech Syst Signal Pr* **40**(2): 791–804 (2013)

[23] Brethee K F, Ma J J, Ibrahim G R, Gu F S, Ball A D. Vibration analysis for diagnosis of tribo-dynamic interaction in journal bearings. In: *Proceedings of TEPEN 2022*. Zhang H, Ji Y, Liu T, Sun X, Ball A D, Eds. Berlin (Germany): Springer, 2022: 877–888.

[24] Zhao H, Fu C, Zhang Y Q, Zhu W D, Lu K, Francis E M. Dimensional decomposition-aided metamodels for uncertainty quantification and optimization in engineering: A review. *Comput Method Appl M* **428**: 117098 (2024)

[25] Mohammadpour M, Rahmani R, Rahnejat H. Effect of cylinder deactivation on the tribo-dynamics and acoustic emission of

overlay big end bearings. *P I Mech Eng K—J Mul* **228**(2): 138–151 (2014)

[26] Caesarendra W, Kosasih B, Tieu A K, Zhu H T, Moodie C A S, Zhu Q. Acoustic emission-based condition monitoring methods: Review and application for low speed slew bearing. *Mech Syst Signal Pr* **72**: 134–159 (2016)

[27] Van Hecke B, Qu Y Z, He D. Bearing fault diagnosis based on a new acoustic emission sensor technique. *P I Mech Eng O—J Ris* **229**(2): 105–118 (2015)

[28] Dahmene F, Yaacoubi S, EL Mountassir M. Acoustic emission of composites structures: Story, success, and challenges. *Physcs Proc* **70**: 599–603 (2015)

[29] Hase A L. Early detection and identification of fatigue damage in thrust ball bearings by an acoustic emission technique. *Lubricants* **8**(3): 37 (2020)

[30] Jiang K S, Han L B, Zhou Y Y. Quantitative evaluation of the impurity content of grease for low-speed heavy-duty bearing using an acoustic emission technique. *Meas Control* **52**(7–8): 1159–1166 (2019)

[31] Elforjani M. Estimation of remaining useful life of slow speed bearings using acoustic emission signals. *J Nondestruct Eval* **35**(4): 62 (2016)

[32] Balderston H L. The detection of incipient failure in bearings. *Mater Eval* **27**(6): 121–128 (1969)

[33] Sturm A, Uhlemann D S. Diagnosis of plain bearings by acoustic emission analysis. *Measurement* **3**(4): 185–191 (1985)

[34] Leahy M, Mba D, Cooper P, Montgomery A, Owen D. Experimental investigation into the capabilities of acoustic emission for the detection of shaft-to-seal rubbing in large power generation turbines: A case study. *P I Mech Eng J—J Eng* **220**(7): 607–615 (2006)

[35] Mba D, Rao R B K N. Development of acoustic emission technology for condition monitoring and diagnosis of rotating machines: Bearings, pumps, gearboxes, engines, and rotating structures. *Shock Vib Dig* **38**(1): 3–16 (2006)

[36] Ma J J, Fu C, Zhu W D, Lu K, Yang Y F. Stochastic analysis of lubrication in misaligned journal bearings. *J Tribol* **144**(8): 081802 (2022)

[37] Hase A, Mishina H, Wada M. Correlation between features of acoustic emission signals and mechanical wear mechanisms. *Wear* **292**: 144–150 (2012)

[38] Vencl A, Rac A. Diesel engine crankshaft journal bearings failures: Case study. *Eng Fail Anal* **44**: 217–228 (2014)

[39] Eyre T S. Wear characteristics of metals. *Tribol Int* **9**(5): 203–212 (1976)

[40] Ma J J, Zhang H, Lou S, Chu F L, Shi Z Q, Gu F S, Ball A D. Analytical and experimental investigation of vibration characteristics induced by tribofilm-asperity interactions in hydrodynamic journal bearings. *Mech Syst Signal Pr* **150**: 107227 (2021)

[41] Ma J J, Shi Z Q, Zhang H, Gu F S, Ball A D. An experiment study of acoustic emission generated by dynamic fluid asperity shearing. In: *Proceedings of IncoME-V & CEPE Net-2020*. Zhen D, Wang D, Wang T Y, Wang H J, Huang B S, Sinha J, Ball A D. Eds. Berlin (Germany): Springer, 2021: 14–22.

[42] Mirhadizadeh S A, Esmaili M, Refahi Oskuei A. Development of acoustic emission technology for condition monitoring and diagnosis of journal bearing. In: Proceedings of the Regional Conference of Mechanical Engineering, 2011.

[43] Pao Y H, Gajewski R R, Ceranoglu A N. Acoustic emission and transient waves in an elastic plate. *J Acoust Soc Am* **65**(1): 96–105 (1979)

[44] Mba D. The use of acoustic emission for estimation of bearing defect size. *J Fail Anal Prev* **8**(2): 188–192 (2008)

[45] Al-Ghamd A M, Mba D. A comparative experimental study on the use of acoustic emission and vibration analysis for bearing defect identification and estimation of defect size. *Mech Syst Signal Pr* **20**(7): 1537–1571 (2006)

[46] Jiaa C L, Dornfeld D A. Experimental studies of sliding friction and wear via acoustic emission signal analysis. *Wear* **139**(2): 403–424 (1990)

[47] Wang L, Wood R J K. Acoustic emissions from lubricated hybrid contacts. *Tribol Int* **42**(11–12): 1629–1637 (2009)

[48] Elforjani M, Shanbr S. Prognosis of bearing acoustic emission signals using supervised machine learning. *IEEE T Ind Electron* **65**(7): 5864–5871 (2018)

[49] Zhao H, Zhang Y Q, Zhu W D, Fu C, Lu K. A comprehensive study on seismic dynamic responses of stochastic structures using sparse grid-based polynomial chaos expansion. *Eng Struct* **306**: 117753 (2024)

[50] Kang J X, Lu Y J, Yang X L, Zhao X W, Zhang Y F, Xing Z G. Modeling and experimental investigation of wear and roughness for honed cylinder liner during running-in process. *Tribol Int* **171**: 107531 (2022)

[51] Vakis A I, Yastrebov V A, Scheibert J, Nicola L, Dini D, Minfray C, Almqvist A, Paggi M, Lee S, Limbert G, et al. Modeling and simulation in tribology across scales: An overview. *Tribol Int* **125**: 169–199 (2018)

[52] Mokhtari N, Rahbar F, Gühmann C. Differentiation of journal bearing friction states and friction intensities based on feature extraction methods applied on acoustic emission signals. *Tech Mess* **84**(s1): 42–47 (2017)

[53] Ziegler B. Contribution of acoustic emission into optimal bearing lubrication. *J Kones* **14**: 571–578 (2007)

[54] Baranov V M, Kudryavtsev E M, Sarychev G A. Modelling of the parameters of acoustic emission under sliding friction of solids. *Wear* **202**(2): 125–133 (1997)

[55] Ma J J, Zhang H, Shi Z Q, Chu F L, Gu F S, Ball A D. Modelling acoustic emissions induced by dynamic fluid-asperity shearing in hydrodynamic lubrication regime. *Tribol Int* **153**: 106590 (2021)

[56] Boness R J, McBride S L, Sobczyk M. Wear studies using acoustic emission techniques. *Tribol Int* **23**(5): 291–295 (1990)

[57] Ziegler B, Wierzcholski K, Miszczak A. Friction forces measurements by the acoustic emission for slide bearing test stand in uni of applied science Giessen. *J Kones* **15**: 627–633 (2008)

[58] Couturier J, Mba D. Operational bearing parameters and acoustic emission generation. *J Vib Acoust* **130**(2): 024502 (2008)

[59] Ziegler B, Wierzcholski K, Miszczak A. A new method of measuring the operating parameters of slide journal bearings by using acoustic emission. *Tribologia* (6a228): 165–173 (2009)

[60] Albers A, Dickerhof M. Simultaneous monitoring of rolling-element and journal bearings using analysis of structure-born ultrasound acoustic emissions. In: Proceedings of the ASME International Mechanical Engineering Congress and Exposition, Vancouver, Canada, 2010: 247–255.

[61] Nagata M, Fujita M, Yamada M, Kitahara T. Evaluation of tribological properties of bearing materials for marine diesel engines utilizing acoustic emission technique. *Tribol Int* **46**(1): 183–189 (2012)

[62] Bergmann P, Grün F, Summer F, Gódor I, Stadler G. Expansion of the metrological visualization capability by the implementation of acoustic emission analysis. *Adv Tribol* **2017**: 3718924 (2017)

[63] Schnabel S, Golling S, Marklund P, Larsson R. The influence of contact time and event frequency on acoustic emission signals. *P I Mech Eng J—J Eng* **231**(10): 1341–1349 (2017)

[64] Hu S T, Huang W F, Shi X, Peng Z K, Liu X F. Mechanism of bi-Gaussian surface topographies on generating acoustic emissions under a sliding friction. *Tribol Int* **131**: 64–72 (2019)

[65] Poddar S, Tandon N. Classification and detection of cavitation, particle contamination and oil starvation in journal bearing through machine learning approach using acoustic emission signals. *P I Mech Eng J—J Eng* **235**(10): 2137–2143 (2021)

[66] Towsyfyan H, Raharjo P, Gu F, Ball A D. Characterization of acoustic emissions from journal bearings for fault detection. In: Proceedings of the Materials Testing, 2013.

[67] Moshkovich A, Perfilyev V, Lapsker I, Feldman Y, Rapoport L. Study of the transition from EHL to BL regions under friction of Ag

and Ni. I. Analysis of acoustic emission. *Tribol Int* **113**: 189–196 (2017)

[68] Raharjo P. An investigation of surface vibration, airbourne sound and acoustic emission characteristics of a journal bearing for early fault detection and diagnosis. Ph.D. Thesis. Hudersfiled (UK): University of Huddersfiled, 2013.

[69] Poddar S, Tandon N. Characteristics of acoustic emission signal for fault diagnosis of journal bearing. In: Proceedings of the International Conference on Condition Monitoring, 2016.

[70] Towsyfyan H, Gu F S, Ball A D, Liang B. Tribological behaviour diagnostic and fault detection of mechanical seals based on acoustic emission measurements. *Friction* **7**(6): 572–586 (2019)

[71] Wei N S, Gu J X, Gu F S, Chen Z, Li G X, Wang T, Ball A D. An investigation into the acoustic emissions of internal combustion engines with modelling and wavelet package analysis for monitoring lubrication conditions. *Energies* **12**(4): 640 (2019)

[72] Lingard S, Ng K K. An investigation of acoustic emission in sliding friction and wear of metals. *Wear* **130**(2): 367–379 (1989)

[73] Fan Y B, Gu F S, Ball A D. Modelling acoustic emissions generated by sliding friction. *Wear* **268**(5–6): 811–815 (2010)

[74] Mirhadizadeh A S, Mba D. Observations of acoustic emission in a hydrodynamic bearing. *J Qual Maint Eng* **15**(2): 193–201 (2009)

[75] Raharjo P, Gu J, Fan Y, Gu F S, Ball A D. Early failure detection and diagnostics of self-aligning journal bearing through vibro-acoustic analysis. In: Proceedings of the 7th International Conference on Condition Monitoring and Machinery Failure Prevention Technologies, 2010.

[76] Ziegler B, Wierzcholski K, Miszczak A. Friction forces measurements for slide bearing test stand in Maritime University Gdynia using the acoustic emission method. *J Kones* **15**: 571–577 (2008)

[77] Ziegler B, Wierzcholski K, Miszczak A. A new measurement method of friction forces regarding slide journal bearings by acoustic emission. *Tribologia* **229**(1): 149–156 (2010)

[78] Saeidi F, Shevchik S A, Wasmer K. Automatic detection of scuffing using acoustic emission. *Tribol Int* **94**: 112–117 (2016)

[79] Borghesani P, Smith W A, Zhang X, Feng P, Antoni J, Peng Z. A new statistical model for acoustic emission signals generated from sliding contact in machine elements. *Tribol Int* **127**: 412–419 (2018)

[80] Hutt S, Clarke A, Evans H P. Generation of Acoustic Emission from the running-in and subsequent micropitting of a mixed-elastohydrodynamic contact. *Tribol Int* **119**: 270–280 (2018)

[81] Gutierrez R, Fang T S, Mainwaring R, Reddyhoff T. Predicting the coefficient of friction in a sliding contact by applying machine learning to acoustic emission data. *Friction* **12**(6): 1299–1321 (2024)

[82] Wang X W. Study of acoustic emission on rubbing impact fault diagnosis of rotating machines. Ph.D. Thesis. Harbin (China): Harbin Institute of Technology, 2009.

[83] Wang Q, Chu F. Experimental determination of the rubbing location by means of acoustic emission and wavelet transform. *J Sound Vib* **248**(1): 91–103 (2001)

[84] Hisakado T, Warashina T. Relationship between friction and wear properties and acoustic emission characteristics: Iron pin on hardened bearing steel disk. *Wear* **216**(1): 1–7 (1998)

[85] Eftekharnejad B, Carrasco M R, Charnley B, Mba D. The application of spectral kurtosis on Acoustic Emission and vibrations from a defective bearing. *Mech Syst Signal Pr* **25**(1): 266–284 (2011)

[86] Zhang G H, Liu Z S, Wang X W, Xu H J. Experimental study of tilting pad journal bearing—Rotor system with acoustic emission technique. *P I Mech Eng J—J Eng* **224**(1): 115–122 (2010)

[87] Raharjo P, Abdusslam S A, Wang T, Gu F S, Ball A D. An investigation of acoustic emission responses of a self aligning spherical journal bearing. In: Proceedings of the Eighth International Conference on Condition Monitoring and Machinery Failure Prevention Technologies, 2011: 424–439.

[88] Gesella G, Murawski L. The influence of changes in the rotational speed of the shaft journal slide bearing on the acoustic emission signal. *J Kones Powertrain Transp* **23**(2): 121–128 (2016)

[89] Mirhadizadeh S A, Moncholi E P, Mba D. Influence of operational variables in a hydrodynamic bearing on the generation of acoustic emission. *Tribol Int* **43**(9): 1760–1767 (2010)

[90] Lei Y G, He Z J, Zi Y Y, Chen X F. New clustering algorithm-based fault diagnosis using compensation distance evaluation technique. *Mech Syst Signal Pr* **22**(2): 419–435 (2008)

[91] Binsaeid S, Asfour S, Cho S, Onar A. Machine ensemble approach for simultaneous detection of transient and gradual abnormalities in end milling using multisensor fusion. *J Mater Process Tech* **209**(10): 4728–4738 (2009)

[92] Shanbhag V V, Meyer T J J, Caspers L W, Schlanbusch R. Defining acoustic emission-based condition monitoring indicators for monitoring piston rod seal and bearing wear in hydraulic cylinders. *Int J Adv Manuf Technol* **115**: 2729–2746 (2021)

[93] Phinyomark A, Thongpanja S, Hu H S, Phukpattaranont P, Limsakul C. The usefulness of mean and median frequencies in electromyography analysis. In: *Computational Intelligence in Electromyography Analysis—A Perspective on Current Applications and Future Challenges*. Naik G R, Ed. London (UK): InTechOpen, 2012: 195–220.

[94] Inayatullah O, Jamaludin N, Ali A, Mohd Nor M J. Application of acoustic emission technique to observer the engine oil's viscosity. In: Proceedings of the 2nd International Conference on Instrumentation Control and Automation, 2011: 344–348.

[95] Raharjo P, Tesfa B, Gu F S, Ball A D. A comparative study of the monitoring of a self aligning spherical journal using surface vibration, airborne sound and acoustic emission. *J Phys Conf Ser* **364**: 012035 (2012)

[96] Raharjo P, Abdusslam S A, Gu F S, Ball A D. Vibro-acoustic characteristic of a self aligning spherical journal bearing due to eccentric bore fault. In: Proceedings of the 9th International Conference on Condition Monitoring and Machinery Failure Prevention Technologies, 2012: 124–140.

[97] Yu Y, Yang P. Research of acoustic emission characteristics based on the signal parameters. In: Proceedings of the International Conference on Information Engineering and Computer Science, 2009: 1–4.

[98] Bote-Garcia J L, Mokhtari N, Gühmann C. Wear monitoring of journal bearings with acoustic emission under different operating conditions. In: Proceedings of the 5th European Conference of the Prognostics and Health Management Society, 2020.

[99] Poddar S, Tandon N. Detection of journal bearing vapour cavitation using vibration and acoustic emission techniques with the aid of oil film photography. *Tribol Int* **103**: 95–101 (2016)

[100] Sun J, Wood R J K, Wang L, Care I, Powrie H E G. Wear monitoring of bearing steel using electrostatic and acoustic emission techniques. *Wear* **259**(7–12): 1482–1489 (2005)

[101] Burger W, Albers A, Scovino R, Dickerhof M. Acoustic emission analysis for monitoring of tribological systems. In: Proceedings of the World Tribology Congress III, 2005: 849–850.

[102] Baran I, Nowak M, Darski W. Application of acoustic emission in monitoring of failure in slide bearings. *J Acoust Emiss* **25**: 341–347 (2007)

[103] Mokhtari N, Pelham J G, Nowoisky S, Bote-Garcia J L, Gühmann C. Friction and wear monitoring methods for journal bearings of geared turbofans based on acoustic emission signals and machine learning. *Lubricants* **8**(3): 29 (2020)

[104] Renhart P, Maier M, Strablegg C, Summer F, Grün F, Eder A. Monitoring tribological events by acoustic emission measurements for bearing contacts. *Lubricants* **9**(11): 109 (2021)

[105] Hosseini S, Najafabadi M A, Akhlaghi M. The lubrication regimes recognition of a pressure-fed journal bearing by time and frequency domain analysis of acoustic emission signals. *Int J Civ Eng* **13**(2): 59–66 (2019)

[106] Maia L H A, Abrao A M, Vasconcelos W L, Sales W F, Machado A R. A new approach for detection of wear mechanisms and determination of tool life in turning using acoustic emission. *Tribol Int* **92**: 519–532 (2015)

[107] Wada M, Mizuno M, Sasada T. Study on the in-process measurement of the friction and wear with AE technique. monitoring of seizure process through AE analysis. *J Jpn S Prec Eng* **56**(10): 1835–1840 (1990)

[108] Ramadan S, Gaillet L, Tessier C, Idrissi H. Detection of stress corrosion cracking of high-strength steel used in prestressed concrete structures by acoustic emission technique. *Appl Surf Sci* **254**(8): 2255–2261 (2008)

[109] Yang L, Zhou Y C. Wavelet analysis of acoustic emission signals from thermal barrier coatings. *T Nonferr Metal Soc* **16**: s270–s275 (2006)

[110] Chang H, Han E H, Wang J Q, Ke W. Acoustic emission study of fatigue crack closure of physical short and long cracks for aluminum alloy LY12CZ. *Int J Fatigue* **31**(3): 403–407 (2009)

[111] Chung K H, Oh J K, Moon J T, Kim D E. Particle monitoring method using acoustic emission signal for analysis of slider/disk/particle interaction. *Tribol Int* **37**(10): 849–857 (2004)

[112] Wada M, Mizuno M. Study on friction and wear utilizing acoustic emission. Relation between friction and wear mode and acoustic emission signals. *J Jpn S Prec Eng* **55**(4): 673–678 (1989)

[113] Baranov V M, Kudryavtsev E M, Sarychev G A, Schavelin V M. *Acoustic Emission in Friction*. Amsterdam (the Netherlands): Elsevier Science, 2011.

[114] Ferrer C, Salas F, Pascual M, Orozco J. Discrete acoustic emission waves during stick–slip friction between steel samples. *Tribol Int* **43**(1–2): 1–6 (2010)

[115] Savchenko N L, Filippov A V, Tarasov S Y, Dmitriev A I, Shilko E V, Grigoriev A S. Acoustic emission characterization of sliding wear under condition of direct and inverse transformations in low-temperature degradation aged Y-TZP and Y-TZP–Al_2O_3. *Friction* **6**(3): 323–340 (2018)

[116] Chen P, Chua P S K, Lim G H. A study of hydraulic seal integrity. *Mech Syst Signal Pr* **21**(2): 1115–1126 (2007)

[117] Shiroishi J, Li Y, Liang S, Kurfess T, Danyluk S. Bearing condition diagnostics via vibration and acoustic emission measurements. *Mech Syst Signal Pr* **11**(5): 693–705 (1997)

[118] Sreedhar P, Balasubramanian K. Acoustic emission monitoring of lube oil condition in large IC engines. In: Proceedings of the 18th World Conference on Nondestructive Testing, 2012.

[119] Hase A, Mishina H, Wada M. Fundamental study on early detection of seizure in journal bearing by using acoustic emission technique. *Wear* **346**: 132–139 (2016)

[120] Poddar S, Tandon N. Study of oil starvation in journal bearing using acoustic emission and vibration measurement techniques. *J Tribol* **142**(12): 121801 (2020)

[121] He Y Y, Yin X Y, Chu F L. Modal analysis of rubbing acoustic emission for rotor-bearing system based on reassigned wavelet scalogram. *J Vib Acoust* **130**(6): 061009 (2008)

[122] Deshpande P, Pandiyan V, Meylan B, Wasmer K. Acoustic emission and machine learning based classification of wear generated using a pin-on-disc tribometer equipped with a digital holographic microscope. *Wear* **476**: 203622 (2021)

[123] Sadegh H, Mehdi A N, Mehdi A. Classification of acoustic emission signals generated from journal bearing at different lubrication conditions based on wavelet analysis in combination with artificial neural network and genetic algorithm. *Tribol Int* **95**: 426–434 (2016)

[124] König F, Jacobs G, Stratmann A, Cornel D. Fault detection for sliding bearings using acoustic emission signals and machine learning methods. *IOP Conf Ser—Mater Sci Eng* **1097**(1): 012013 (2021)

[125] König F, Sous C, Ould Chaib A, Jacobs G. Machine learning based anomaly detection and classification of acoustic emission events for wear monitoring in sliding bearing systems. *Tribol Int* **155**: 106811 (2021)

[126] König F, Marheineke J, Jacobs G, Sous C, Zuo M J, Tian Z G. Data-driven wear monitoring for sliding bearings using acoustic emission signals and long short-term memory neural networks. *Wear* **476**: 203616 (2021)

[127] Mokhtari N, Gühmann C. Classification of journal bearing friction states based on acoustic emission signals. *Tech Mess* **85**(6): 434–442 (2018)

[128] Bin G F, Liao C J, Li X J. The method of fault feature extraction from acoustic emission signals using Wigner-Ville distribution. *Adv Mat Res* **216**: 732–737 (2011)

[129] He P, Li P, Sun H Q. Feature extraction of acoustic signals based on complex morlet wavelet. *Procedia Engineer* **15**: 464–468 (2011)

[130] Kilundu B, Chiementin X, Duez J, Mba D. Cyclostationarity of acoustic emissions (AE) for monitoring bearing defects. *Mech Syst Signal Pr* **25**(6): 2061–2072 (2011)

[131] Lin T R, Kim E, Tan A C C. A practical signal processing approach for condition monitoring of low speed machinery using Peak-Hold-Down-Sample algorithm. *Mech Syst Signal Pr* **36**(2): 256–270 (2013)

[132] Oh H, Azarian M H, Pecht M G. Estimation of fan bearing degradation using acoustic emission analysis and mahalanobis distance. In: Proceedings of MFPT: The Applied Systems Health Management Conference, 2011.

[133] Matsuoka K, Forrest D, Ming-Kai T. On-line wear monitoring using acoustic emission. *Wear* **162**: 605–610 (1993)

[134] Hu S T, Huang W F, Shi X, Peng Z K, Liu X F, Wang Y M. Bi-Gaussian stratified effect of rough surfaces on acoustic emission under a dry sliding friction. *Tribol Int* **119**: 308–315 (2018)

[135] Hu S T, Brunetiere N, Huang W F, Liu X F, Wang Y M. Stratified revised asperity contact model for worn surfaces. *J Tribol* **139**(2): 021403 (2017)

[136] Hu S T, Huang W F, Brunetiere N, Song Z X, Liu X F, Wang Y M. Stratified effect of continuous bi-Gaussian rough surface on lubrication and asperity contact. *Tribol Int* **104**: 328–341 (2016)

[137] Hao Q S, Shen Y, Wang Y, Zhang X. A fractal model of acoustic emission signals in sliding friction. *Tribol Lett* **67**: 31 (2019)

[138] Greenwood J A, Williamson J B P. Contact of nominally flat surfaces. *Proc R Soc Lond A* **295**(1442): 300–319 (1966)

[139] Towsyfyan H, Gu F S, Ball A D, Liang B. Modelling acoustic emissions generated by tribological behaviour of mechanical seals for condition monitoring and fault detection. *Tribol Int* **125**: 46–58 (2018)

[140] Ma J J, Fu C, Zhang H, Chu F L, Shi Z Q, Gu F S, Ball A D. Modelling non-Gaussian surfaces and misalignment for condition monitoring of journal bearings. *Measurement* **174**: 108983 (2021)

Jiaojiao Ma obtained her Ph.D. degree from Hebei University of Technology, China. She is a graduate supervisor and associate professor at Foshan University, China. Her research interests include machine dynamics, fluid tribology dynamic responses, signal processing, condition monitoring, and fault diagnosis.

Jiefei Yu is a master candidate at the School of Mechanical and Electrical Engineering and Automation, Foshan University, China. His current research interests include AE signal processing, condition monitoring, and fault diagnosis of lubricant journal bearings.

Xianwen Zhou received his Ph.D. degree from Dalian University of Technology, China. He is a graduate supervisor at Foshan University, China. His research interests include machinery condition monitoring, fault diagnosis, tribology, and advanced signal processing techniques.

Lingli Jiang received her Ph.D. degree from Central South University, China, in 2010. She is a graduate supervisor and distinguished professor at Foshan University, China. Her research interests include machinery condition monitoring, fault detection and diagnosis, and machine dynamics.

Fengshou Gu is an expert in vibro-acoustics analysis and machinery diagnosis, with over 30 years of research experience. Now, he is a professor at the University of Huddersfield, UK. His research interests include machine dynamics, advanced signal processing techniques, tribology dynamic responses, condition monitoring measurement systems, sensor development artificial intelligence, and related fields.

Xuejun Li is a professor at the School of Mechanical and Electrical Engineering and Automation, Foshan University, China. His research interests include mechanical transmission, machine dynamics, machinery health management, and intelligent maintenance.